

1 Tracing the migration of mantle CO₂ in gas fields and mineral water
2 springs in south-east Australia using noble gas and stable isotopes

3 **This manuscript has been submitted for publication in *Geochimica et Cosmochimica***
4 **Acta. This is the non peer-reviewed original version. The final version of the**
5 **manuscript will be available via the 'Peer-reviewed Publication DOI' link on the right-**
6 **hand side of the webpage.**

7

8

9 Rūta Karolytė^{1*}, Gareth Johnson¹, Domokos Györe², Sascha Serno¹, Stephanie Flude¹, Finlay M.

10 Stuart², Allan R. Chivas^{3,4}, Adrian Boyce² and Stuart M.V. Gilfillan¹

11 ¹School of GeoSciences, University of Edinburgh, James Hutton Road, Edinburgh, EH9 3FE, UK

12 ²Isotope Geoscience Unit, Scottish Universities Environmental Research Centre (SUERC), East

13 Kilbride, G75 0QF, UK

14 ³GeoQuEST Research Centre, School of Earth and Environmental Sciences, University of Wollongong,

15 Wollongong, NSW 2522, Australia

16 ⁴Department of Earth Sciences and Sprigg Geobiology Centre, The University of Adelaide SA 5005,

17 Australia

18 *Author for correspondence: ruta.karolyte@ed.ac.uk

19 Keywords: Carbon Capture and Storage; geochemical tracing; noble gases; carbon isotopes; helium;

20 mantle; CO₂ springs; solubility fractionation; Otway Basin.

21 **Abstract**

22 Geochemical monitoring of CO₂ storage requires understanding of both innate and introduced fluids
23 in the crust as well as the subsurface processes that can change the geochemical fingerprint of CO₂
24 during injection, storage and any subsequent migration. Here, we analyse a natural analogue of CO₂
25 storage, migration and leakage to the atmosphere, using noble gas and stable isotopes to constrain
26 the effect of these processes on the geochemical fingerprint of the CO₂. We present the most
27 comprehensive evidence to date for mantle-sourced CO₂ in south-east Australia, including well gas
28 and CO₂-rich mineral spring samples from the Otway Basin and Central Victorian Highlands (CVH).
29 ³He/⁴He ratios in well gases and CO₂ springs range from 1.21 to 3.07 R_A and 1.23 – 3.65 R_C/R_A,
30 respectively. We present chemical fractionation models to explain the observed range of ³He/⁴He
31 ratios, He, Ne, Ar, Kr, Xe concentrations and δ¹³C(CO₂) values in the springs and the well gases. The
32 variability of ³He/⁴He in the well gases is controlled by the gas residence time in the reservoir and
33 associated radiogenic ⁴He accumulation. ³He/⁴He in CO₂ springs decrease away from the main
34 mantle fluid supply conduit. We identify one main pathway for CO₂ supply to the surface in the CVH,
35 located near a major fault zone. A new solubility fractionation model, describing noble gas

36 partitioning between water and gas at the shallow surface during bubble formation, is proposed to
37 explain the range in noble gas concentrations and $\delta^{13}\text{C}(\text{CO}_2)$ values measured in the mineral spring
38 samples. This process is also responsible for low ^3He concentrations and associated high $\text{CO}_2/^3\text{He}$,
39 which are commonly interpreted as evidence for mixing with crustal CO_2 . The elevated $\text{CO}_2/^3\text{He}$ can
40 be explained solely by solubility fractionation without the need to invoke other CO_2 sources. The
41 noble gases in the springs and well gases can be traced back to a single end-member which has
42 suffered varying degrees of radiogenic helium accumulation and late stage degassing. This work
43 shows that combined stable and noble gas isotopes in natural gases provide a robust tool for
44 identifying the migration of injected CO_2 to the shallow subsurface.
45

46 1. Introduction

47 The development of geochemical tracing techniques to ascertain the origin and genetic link
48 between natural gases trapped in subsurface reservoirs and those degassing at the surface is
49 important to the safe and successful deployment of carbon capture and storage (CCS). Safe disposal
50 of captured industrial CO_2 requires verification of the fate of the injected gas and reassurance that
51 injected gas does not migrate to the surface (IPCC, 2005). To ensure this, CCS operators have to
52 adhere to legislative guidelines and verify that injected CO_2 is securely contained within the reservoir
53 formation (Dixon et al., 2015). While a variety of geophysical, geoelectric and thermal sensing
54 monitoring techniques exist (Giese et al., 2009), the high sensitivity of geochemical monitoring
55 techniques is useful for detecting seepage at low concentrations, verifying gas origin and tracing the
56 interactions between different crustal fluids (Myers et al., 2013; Stalker and Myers, 2014; Roberts et
57 al., 2017).

58 The noble gas isotopes have previously been applied in an engineered setting to assess CO_2
59 migration, dissolution and residual trapping in reservoir pore spaces at the Cranfield CO_2 -EOR site
60 field (Györe et al., 2015; Györe et al., 2017) and to study industrial underground natural gas storage
61 in the Paris Basin (Jeandel et al., 2010). Noble gas tracers have been used to refute allegations of
62 injected CO_2 leakage to the surface near the Weyburn-Midale CO_2 Monitoring and Storage Project
63 (Gilfillan et al., 2017) and to identify fugitive gas migration to shallow aquifers caused by industrial
64 hydraulic fracturing operations (Darrah et al., 2014). The techniques used in these industrial studies
65 have been informed by preceding research of natural gas fields and springs (e.g. Ballentine and
66 O’Nions, 1994; Gilfillan et al., 2014, 2009, 2008; Sherwood Lollar et al., 1997; Wilkinson et al., 2009).
67 Natural analogue studies remain a crucial gateway to developing geochemical tracing methods for
68 the industrial sector, providing information about fluid migration and retention processes occurring
69 over geological time scales (Baines and Worden, 2004; Haszeldine et al., 2005; Holland and Gilfillan,
70 2013).

71 Helium is an unrivalled indicator of crustal fluid migration in the subsurface because it is
72 sensitive to changes in the balance between volatiles derived from the mantle and the crust. This is
73 because the original helium composition of any subsurface fluid is not significantly modified by
74 interaction with groundwater due to the low abundance of helium in the atmosphere (Ozima and
75 Podosek, 2002). Hence, helium is particularly applicable to tracing gas migration through a water
76 system in both natural and industrial fugitive gas migration monitoring settings. Here we draw from
77 existing methodologies of helium use in tracing the migration of mantle fluids (Sano et al., 1990;
78 Sakamoto et al., 1992), mixing of different fluid sources (O’Nions and Oxburgh, 1988; Sano and
79 Marty, 1995) and dating natural gas and groundwater resources (Zhou and Ballentine, 2006; Liu et
80 al., 2016) to provide a comprehensive account on the geochemical link between natural CO₂ gases,
81 trapped in the subsurface and emanating in the shallow surface.

82 Noble gases are soluble in water and partition according to their relative solubilities during
83 gas-water equilibration. This property has been utilised mainly in assessing reservoir-scale water-gas
84 equilibration and gas migration or groundwater recharge conditions (Bosch and Mazor, 1988;
85 Ballentine et al., 1996; Barry et al., 2016) and the presence of ‘excess air’ above the atmospheric
86 solubility equilibrium (Aeschbach-Hertig et al., 2008; Kipfer et al., 2002). The former is largely based
87 on atmospheric noble gas ratios, whilst the latter combines ratios with elemental concentrations.
88 Atmospheric noble gas ratios in CO₂ springs are commonly similar to air saturated water (ASW) and
89 the utility of these noble gases is often overlooked. We discuss the use of noble gas concentration
90 data in assessing the solubility fractionation effects of near-surface degassing and reconstructing the
91 original noble gas composition for the purpose of tracing.

92 The physical and chemical processes contributing to and modifying the noble gas contents of
93 CO₂ are explored using the data from three natural CO₂ fields in the Otway Basin of SE Australia and
94 ten natural CO₂-rich springs in Victoria. We focus on identifying the origin of the gases and the
95 genetic link between gases stored in reservoir traps and those emanating at the surface from the
96 natural mineral springs.

97 2 Geological setting

98 2.1 Basin setting and location of CO₂ gas fields and springs

99 The Otway Basin developed along the southern Australian margin as a result of crustal
100 extension due to sea floor spreading between Australia and Antarctica. The sedimentary section of
101 the basin comprises Upper Jurassic – Lower Cretaceous Otway Group sediments (Bernecker and
102 Moore, 2003). The present geometry of the basin is characterised by NW-SE trending normal faults,

103 and was established during Jurassic to Cretaceous rifting and subsequent reactivation during a short-
104 lived period of basin inversion in the Miocene (Cox et al., 1995; Teasdale et al., 2003).

105 The basement comprises Lachlan and Delamerian fold belts, separated by the Moyston
106 lithospheric suture which extends to the Moho (Fig. 1a). Parallel N-S trending large-scale shear zones
107 and reverse faults connect to the Moyston Fault at depth (Fig. 1d) (Cayley et al., 2011). The structure
108 of the Otway Basin has been strongly controlled by the fabric of the underlying basement. Old
109 basement structures have a significant rheology contrast along them and are more likely to undergo
110 structural reactivation during a change in the stress regime (Hand and Sandiford, 1999). The Jurassic-
111 Cretaceous extension was mainly accommodated along structural weaknesses of the basement,
112 which created graben and half-graben structures favourable for fluid trapping. Hydrocarbons and
113 CO₂ discoveries in the Otway Basin therefore tend to coincide with the location of deep basement
114 faults (Bernecker and Moore, 2003).

115 The basin contains numerous accumulations of CO₂, methane and other hydrocarbons in
116 varying concentrations (Boult et al., 2004). The three gas fields investigated in this work contain CO₂
117 concentrations above 75 mol %, with the remainder of the gas content being primarily methane. The
118 Caroline field is located in South Australia, near Mt Gambier and is a commercially explored CO₂ field
119 which has a CO₂ concentration in excess of 98 % (Chivas et al., 1987). Boggy Creek and Buttress fields
120 are located in the Port Campbell Embayment at the eastern side of the Otway Basin (Boreham et al.,
121 2011). Methane generation is dated to mid-Paleogene (Duddy, 1997), followed by a later-stage CO₂
122 emplacement (Boult et al., 2004; Watson et al., 2004; Lyon et al., 2005).

123 CO₂-rich mineral spring waters emanate at the ground surface within the extent and north of
124 the basin. Over a hundred ambient temperature mineral springs are located in the Central Victorian
125 Highlands (CVH) (Fig. 1b). Mineral water flows through a fracture-dominated aquifer consisting of
126 Ordovician low-grade metasedimentary sequence and discharges into topographic lows such as
127 streambeds. Many of the springs also release CO₂ and can be identified as degassing CO₂ bubble
128 trails into creek beds or standing pools of water. Springs are clustered along the Muckleford Fault,
129 which is a deep Proterozoic reverse fault extending down to the lower crust and connecting to the
130 Moyston suture zone (Cayley et al., 2011) (Fig. 1d).

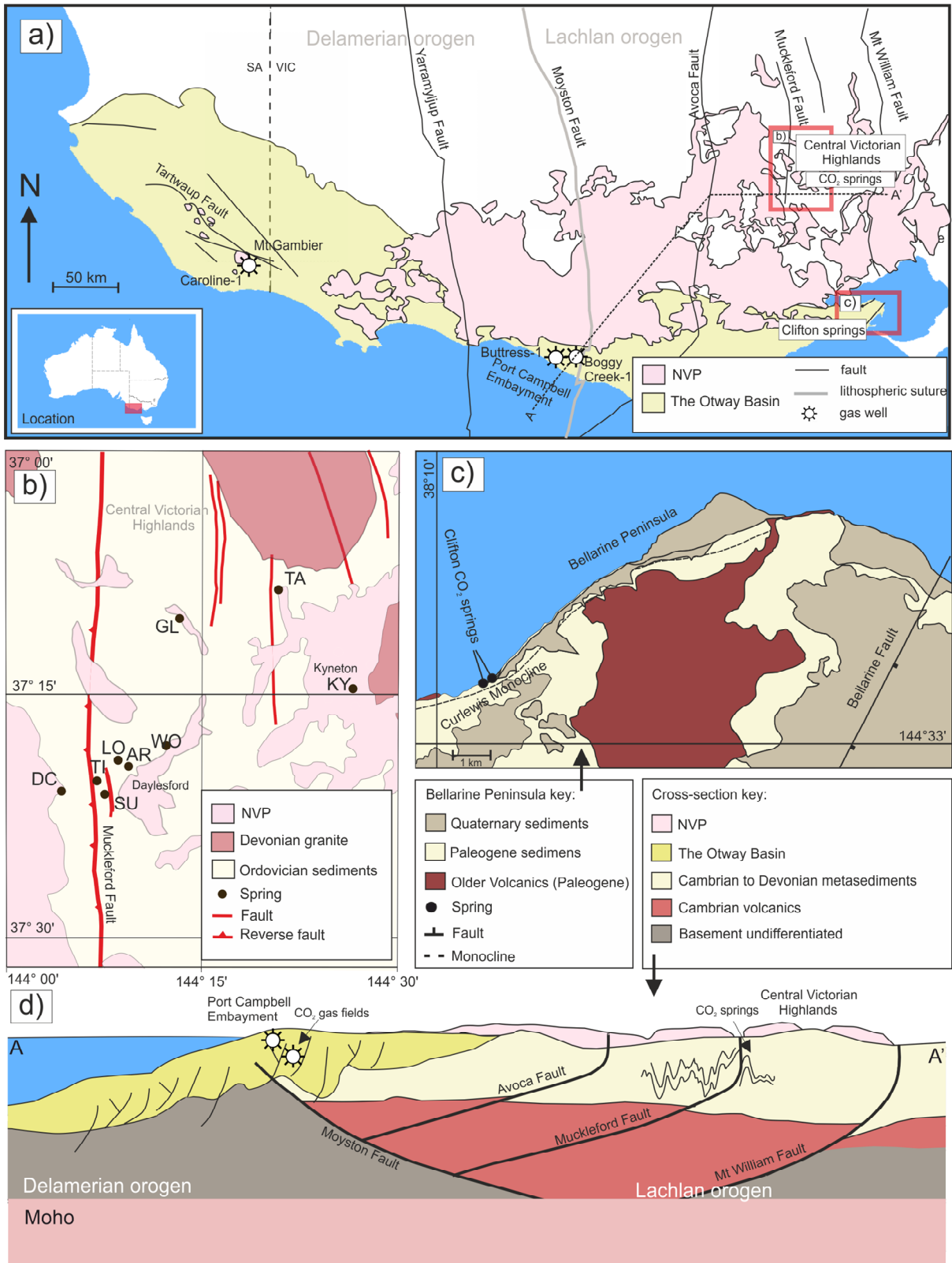
131 Mineral springs also emerge on the northern coast of Bellarine Peninsula, at Clifton Springs
132 near Geelong, on the south-eastern edge of the Otway Basin (Fig. 1c). The central part of the
133 Bellarine Peninsula has been uplifted in the late Miocene during the inversion of NE-SW trending
134 normal faults (Coulson, 1933). The north coast of the peninsula is structurally controlled by the

135 Curlewis Monocline, underlain by a south dipping normal fault. The Curlewis Monocline is parallel to
136 the structural lineaments of the basement and could be associated with deeper basement faults
137 (Dahlhaus, 2003). CO₂ springs emerge along the shoreline parallel to the fault.

138 The basement and the Otway Basin are overlain by the Newer Volcanic Province (NVP)
139 extrusives that stretch from the CVH to the northern edges of the Port Campbell Embayment. The
140 province is a well preserved intra-plate basaltic lava field with more than 400 eruptive centres
141 (Boyce, 2013), active between 5 Ma and 4.5 ka (Cas et al., 2017). The last eruption dated at 4.5 ka,
142 occurred at Mount Gambier, located near the Caroline CO₂ field (Robertson et al., 1996). Many of
143 the oldest eruptive centres are found in the eastern side of the province and near the CVH (4.6 - 2.6
144 Ma) (Price et al., 1997), but no systematic pattern of eruptions ages exists (Cas et al., 2017). There is
145 no evidence for volcanic activity of this period in the Bellarine Peninsula where Clifton Springs are
146 located, although The Older Volcanics (39 - 49 Ma) crop out in the area (Price et al., 1997). The cause
147 of the recent volcanism is currently unresolved. Common theories include a mantle plume (Wellman
148 and McDougall, 1974; Wellman, 1983), edge-driven isolated mantle convection (King and Anderson,
149 1998), batch-melting caused by fault reactivation (Lesti et al., 2008), or a combination of all these
150 factors (Demidjuk et al., 2007; Davies and Rawlinson, 2014).

151 2.2 Previous noble gas studies of the gas fields and CO₂ springs

152 Despite the commercial exploration of CO₂ gas fields in the Otway Basin and springs in the
153 CVH, studies of the CO₂ origins have been limited and the processes associated with the gas
154 migration in the subsurface and to the surface are poorly understood. Chivas et al. (1987) reported
155 ³He/⁴He values of up to 3.1 R_A in the Caroline field and Caffee et al. (1999) identified the presence of
156 primordial Xe in the field, providing evidence for a mantle source. Mantle helium has also been
157 reported in the Lavers-1 gas field in the Otway Basin (1.68 R/R_A) (Watson et al., 2004). Preliminary
158 ³He/⁴He measurements of up to 3.1 R_A have been reported in CO₂ springs at the CVH (Chivas et al.,
159 1983) but no further study has been published. It has been suggested that the source of mantle
160 volatiles in CO₂ springs is associated with the NVP (Lawrence, 1969), however no conclusive evidence
161 currently exists other than geographic proximity to the eruptive centres. Prior to this work no
162 geochemical study into the origin of the CO₂ degassing at the Bellarine Peninsula had been
163 published.



164

165 **Figure 1. Location map of the studied CO₂ gas fields and springs. a) Studied well gases are in two localities in the Otway**
 166 **Basin: Port Campbell Embayment and Mt Gambier. Clifton Springs are located on the eastern edge of the basin. The CVH**
 167 **CO₂ springs emerge from the Ordovician basement rocks in the CVH. The Otway Basin and CVH are dissected by N-S**
 168 **trending faults. The Newer Volcanic province extends across both areas. b) Location of sampled CO₂ springs in CVH;**

169 many of the springs are located near the Muckleford Fault (see Table 1 for sample name abbreviations). c) Clifton
170 Springs are located on the coast of Bellarine Peninsula, along the crest of the Curlewis Monocline. d) Sketch cross-
171 section (not to scale) of A-A' transect on Fig. 1a, showing the structural relationship between the basement and the
172 basin. The Moyston and Mt Williams Faults extend to the Moho. Many of the basement faults (including The Muckleford
173 fault at CVH) are inferred to be connected to the Moyston Fault at depth. Elements of the figure adapted from
174 (Cartwright et al., 2002; Bernecker and Moore, 2003; Watson et al., 2003; Cayley et al., 2011; Cas et al., 2017).

175 2. Methods

176 2.1 CO₂ sampling

177 Gas samples from the natural gas fields in the Otway Basin were collected directly from
178 producing well heads, using 9.5 mm diameter refrigeration grade copper tubing connected to a
179 pressure regulator by plastic hosing. Bubbling gases from the springs were collected using an
180 inverted plastic funnel placed over a bubbling vent, placed into the water column to form an air-tight
181 seal, allowing gas to flow through plastic hose to the copper tube. Tubes were purged for 5 minutes
182 and sealed using two steel clamps specifically manufactured for the purpose of creating a helium
183 leak-tight cold weld seal (Holland and Gilfillan, 2013). Mineral spring water samples were collected
184 via hand pumps, filtered through 0.45 mm pore-size filters and filled into Nalgene bottles. The
185 temperature, pH and TDS of the water in boreholes was measured in the field using a Hanna
186 Instruments HI991300 Portable Waterproof temperature/pH/EC Meter with an accuracy of ± 0.5 °C,
187 ± 0.01 pH and ± 1 $\mu\text{S}/\text{cm}$ for temperature, pH and electrical conductivity respectively. TDS values
188 were obtained from EC measurements using a conversion factor of 0.7 (Walton, 1989).

189 2.2 Laboratory procedures

190 All laboratory work was undertaken at the Scottish Universities Environmental Research
191 Centre (SUERC). Copper tube samples were connected to an all-metal vacuum line, purified using VG
192 Scienta ST22 titanium sublimation pump and ZrAl alloy getter. The isotopic composition of noble
193 gases was measured using a MAP 215-50 mass spectrometer using techniques outlined in Györe et
194 al. (2015). Bulk gas concentrations were measured using a Pfeiffer Vacuum QMS 200 quadrupole
195 mass spectrometer and Hewlett Packard 5890 Series 11 Gas Chromatograph with uncertainties of ± 1
196 $\%$. $\delta^{13}\text{(CO}_2\text{)}$ values were determined using a VG Optima dual inlet isotope ratios mass spectrometer
197 in dynamic mode using an internal standard (Györe et al., 2015). Values are reported relative to
198 VPDB standard with uncertainties of ± 0.2 $\%$.

199 3. Results

200 A total of three well gas and ten spring samples were measured. Sample location, bulk gas
201 composition, $\delta^{13}(\text{CO}_2)$ values, temperature, pH and TDS measurements are reported in Table 1. He,
202 Ne and Ar isotope ratios, and He, Ne, Ar, Kr, Xe concentrations are reported in Table 2. The full suite
203 of noble gases was measured in six of the CO_2 spring samples, while He isotopes were only measured
204 in three well gas and four CO_2 spring samples.

205 **Table 1. Details of the geographic location, bulk gas composition, $\delta^{13}\text{C}(\text{CO}_2)$ values of 3 well gases and 10 CO_2 springs; pH, temperature and TDS measured in water from**
 206 **10 mineral water bores.**

Sample name	Label	Location			Bulk gas composition*							$\delta^{13}\text{C}(\text{CO}_2)$ VPDB	Borehole water		
		Region	Latitude	Longitude	CO_2	CH_4	C_2H_6	C_3H_8	C_4H_{10}	N_2	pH		T °C	TDS g/L	
<i>Well gases</i>															
Caroline-1	CA	Mount Gambier, SA	-37.9417	140.9083	99	0.9	0.01	–	–	0.4	-4.1	–	–	–	
Boggy Creek-1	BC	Port Campbell, VIC	-38.5261	142.8245	87	10.0	0.1	0.03	0.01	2.3	-5.6	–	–	–	
Buttress-1	BU	Port Campbell, VIC	-38.5167	142.8084	77	19.7	0.8	1.1	–	1.9	-7.6	–	–	–	
<i>CO₂ springs</i>															
Taradale	TA	CVH	-37.1393	144.3500	>99						-9.4	6.1	20.9	2.9	
Locarno	LO	CVH	-37.3113	144.1412	>99						-7.2	6.1	16.7	1.6	
Deep Creek	DC	CVH	-37.3419	144.0733	>99						-8.2	5.6	15.7	0.6	
Glenluce	GL	CVH	-37.1623	144.2225	>99	0.1					-7.8	6.3	16.7	2.2	
Woolnoughs	WO	CVH	-37.2942	144.2065	>99						-6.9	6.2	21.1	1.6	
Clifton Springs	CL	Bellarine Peninsula	-38.1510	144.5659	>99						-6.0	5.5	20.5	3.8	
Sutton	SU	CVH	-37.3480	144.1317	>99						-8.4	6.0	19.7	1.1	
Argyle	AR	CVH	-37.3141	144.1553	>99						-9.2	5.8	15.1	1.0	
Kyneton	KY	CVH	-37.2358	144.4200	>99						-8.0 ^a	6.1	18.3	1.2	
Tipperary	TI	CVH	-37.3391	144.1186	>99						-7.1	6.3	16.5	2.2	

207 * Bulk gas composition for Caroline-1 from Chivas et al. (1987), Boggy Creek-1 from Akbari (1992)

208 ^a from Cartwright et al. (2002)

209 **Table 2. Noble gas concentrations and isotopic ratios for 3 well gas samples and 10 CO₂ springs.**

Sample name	³ He/ ⁴ He (R _C /R _A)	²⁰ Ne/ ²² Ne		²¹ Ne/ ²² Ne		⁴⁰ Ar/ ³⁶ Ar		³⁸ Ar/ ³⁶ Ar		⁴ He x 10 ⁻⁶		²⁰ Ne x 10 ⁻⁹		⁴⁰ Ar x 10 ⁻⁵		⁸⁴ Kr x 10 ⁻⁹		¹³² Xe x 10 ⁻¹⁰		
<i>Well gases</i>																				
Caroline-1	3.07	(0.12)	–	–	–	–	–	–	–	96.0	(5.0)	2.2	(0.1)	–	–	–	–	–	–	
Boggy Creek-1	1.21	(0.01)	–	–	–	–	–	–	–	384.4	(18.6)	124.1	(5.3)	–	–	–	–	–	–	
Buttress-1	1.25	(0.01)	–	–	–	–	–	–	–	478.8	(23.2)	15.4	(0.7)	–	–	–	–	–	–	
<i>CO₂ springs</i>																				
Taradale	1.23	(0.03)	9.73	(0.06)	0.030	(0.001)	314	(1)	0.195	(0.008)	4.0	(0.2)	34.3	(1.5)	5.3	(0.2)	8.2	(0.3)	6.9	(0.4)
Locarno	3.14	(0.09)	9.68	(0.05)	0.030	(0.001)	303	(1)	0.191	(0.003)	5.7	(0.2)	59.1	(2.5)	7.8	(0.3)	10.4	(0.43)	6.5	(0.3)
Deep Creek	2.45	(0.07)	9.92	(0.05)	0.029	(0.001)	301	(5)	0.190	(0.003)	8.9	(0.4)	132.3	(5.6)	22.8	(0.8)	39.5	(1.6)	30.4	(1.6)
Glenluce	1.57	(0.07)	9.71	(0.05)	0.028	(0.000)	308	(1)	0.189	(0.003)	163.0	(6.0)	1372	(58)	94.4	(3.5)	63.1	(2.6)	25.6	(1.3)
Woolnoughs	1.71	(0.07)	9.78	(0.06)	0.030	(0.001)	299	(1)	0.190	(0.003)	0.97	(0.04)	1781	(3.7)	86.0	(3.2)	79.9	(3.3)	36.1	(1.9)
Clifton Springs	1.97	(0.06)	9.73	(0.06)	0.029	(0.001)	323	(1)	0.191	(0.003)	42.0	(2.0)	128.8	(5.5)	22.9	(0.8)	29.8	(1.2)	19.9	(1.0)
Sutton	3.14	(0.03)	–	–	–	–	–	–	–	1.61	(0.05)	42.5	(1.5)	–	–	–	–	–	–	–
Argyle	3.65	(0.08)	–	–	–	–	–	–	–	87.9	(2.6)	5502	(196)	–	–	–	–	–	–	–
Kyneton	1.24*	(0.04)	–	–	–	–	–	–	–	4.9	(0.1)	13834	(493)	–	–	–	–	–	–	–
Tipperary	2.70	(0.05)	–	–	–	–	–	–	–	0.48	(0.01)	438.3	(8.9)	–	–	–	–	–	–	–

210 Concentrations are in cm³(STP)/cm³.

211 Errors are 1σ standard deviation.

212 * ³He/⁴He reported uncorrected for atmospheric component due to air contamination

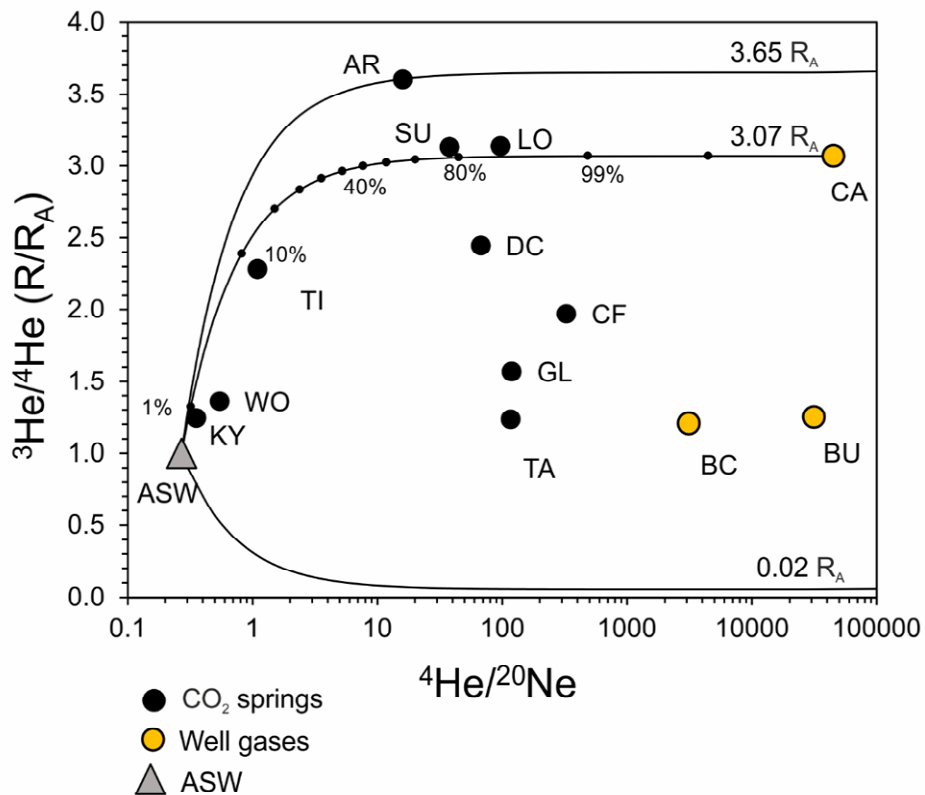
213 3.1. Bulk gas concentrations, $\delta^{13}(\text{CO}_2)$ and water measurements

214 The concentration of CO_2 in the Buttress field is 77 % with the remainder of gas predominately
215 constituting of CH_4 (19.7 %), N_2 (1.9 %) and traces of higher hydrocarbons (0.8 % C_2H_6 , 1.1 % C_3H_{10}).
216 Bulk gas compositions for the other two well gases are taken from the literature. CO_2 concentration
217 in the adjacent Boggy Creek field is slightly higher (87%) (Akbari, 1992). The Caroline field has the
218 highest CO_2 concentrations of 99 % with traces of CH_4 , N_2 and C_2H_6 (Chivas et al., 1987). All mineral
219 spring gas samples were measured to be above 99 % CO_2 with the remainder of gas composed of
220 noble gases. Glenluce is the only spring showing trace amounts of CH_4 (0.1 %). The $\delta^{13}(\text{CO}_2)$ values of
221 the gas samples range from -9.4 to -6 ‰ in springs, and -7.6 to -4.1 ‰ in the well gases. The
222 temperature of the water samples varies from 15.1 – 20.9 °C, pH ranges from 5.8 to 6.3 in CVH
223 springs and 5.5 in Clifton Springs. TDS values range from 0.63 to 2.85 g/L.

224 3.2. Helium and $\text{CO}_2/{}^3\text{He}$ ratios

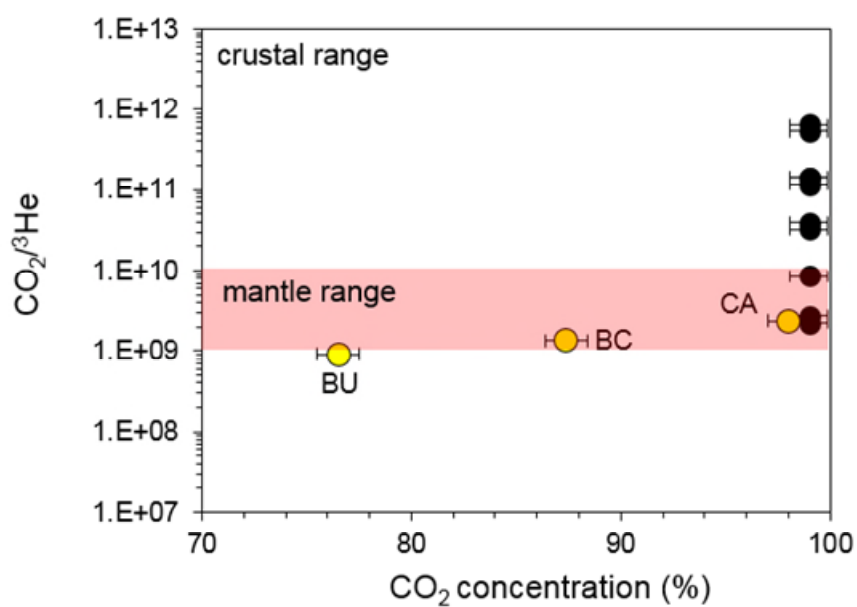
225 ${}^3\text{He}/{}^4\text{He}$ ratios are reported normalised to the value of air (where 1 R_A is the atmospheric ratio
226 of 1.4×10^{-6}). ${}^3\text{He}/{}^4\text{He}$ R_c/R_A are corrected for ${}^4\text{He}$ derived from the atmospheric component, using
227 the ${}^4\text{He}/{}^{20}\text{Ne}$ value of the sample following the methodology in Craig (1978). It is assumed that all
228 ${}^{20}\text{Ne}$ is derived from ASW and the ${}^4\text{He}/{}^{20}\text{Ne}$ value of ASW at 20 °C is 0.27 (Kipfer et al., 2002).
229 ${}^4\text{He}/{}^{20}\text{Ne}$ ratios of the well gases are 4-5 orders of magnitude above the ASW value (3097-44656)
230 and range between 0.35 and 326 in the spring samples. ${}^3\text{He}/{}^4\text{He}$ R_c/R_A values differ significantly from
231 the measured ${}^3\text{He}/{}^4\text{He}$ ratios in spring samples with ${}^4\text{He}/{}^{20}\text{Ne}$ ratios <10 (Woolnoughs and
232 Tipperary). Kyneton is the only sample with significant atmospheric contamination (${}^4\text{He}/{}^{20}\text{Ne} = 0.35$)
233 which would make the correction erroneous (Sano et al., 2006) therefore its ${}^3\text{He}/{}^4\text{He}$ value is
234 reported uncorrected (1.24 R_A). The ${}^3\text{He}/{}^4\text{He}$ ratios of the remaining spring samples range from 1.23
235 to 3.65 R_c/R_A . ${}^3\text{He}/{}^4\text{He}$ ratios of well gases from the Port Campbell region are 1.21 and 1.25 R_A . The
236 sample collected from the Caroline CO_2 field in South Australia exhibits a higher value of 3.07 R_A , in
237 agreement with previous measurements (Chivas et al., 1987). All samples are compatible with two-
238 component mixing in a ${}^3\text{He}/{}^4\text{He}$ vs ${}^4\text{He}/{}^{20}\text{Ne}$ plot, where variable ${}^3\text{He}/{}^4\text{He}$ end-members mix with
239 ASW (Fig. 2).

240 $\text{CO}_2/{}^3\text{He}$ ratios of the well gases are within or below the Mid-Ocean Ridge Basalt (MORB)
241 range of 1×10^9 to 1×10^{10} (Marty and Jambon, 1987). This is quite distinct from the higher $\text{CO}_2/{}^3\text{He}$
242 values predicted for near ${}^3\text{He}$ -free carbonates (O'Nions and Oxburgh, 1988; Sherwood Lollar et al.,
243 1997). CO_2 concentrations in the spring samples are uniform, whilst $\text{CO}_2/{}^3\text{He}$ ratios vary over two
244 orders of magnitude, 2.26×10^9 and 6.5×10^{11} , across the typical mantle and crustal values (Fig. 3).



245

246 Figure 2. $^3\text{He}/^4\text{He}$ R_A plotted against $^4\text{He}/^{20}\text{Ne}$ ratios of springs and well gases. Solid lines depict binary
 247 mixing between ASW and the highest regional mantle end-member (Argyle, $3.65 R_A$), Caroline field and a
 248 crustal end-member ($0.02 R_A$). Black tick marks show percentage of helium from Caroline end-member in
 249 the mixture. Few springs fall close to the mixing line with the Caroline field, the remaining samples have
 250 variable amounts of crustal component. Errors are smaller than the symbols. Abbreviations of sample
 251 names are given in Table 1. Abbreviations of sample names are given in Table 1.



252

253 **Figure 3. CO₂/³He ratios plotted against CO₂ concentrations for the well gases (yellow circles) and CO₂**
254 **springs (black circles). Vertical errors are smaller than the symbols. The shaded area shows the range of**
255 **CO₂/³He values measured in mantle source volatiles (Marty and Jambon, 1987). CO₂/³He ratios above 1 x**
256 **10¹⁰ are typically associated with a crustal CO₂ source (O’Nions and Oxburgh, 1988). Well gas samples are**
257 **within the mantle range but with positive correlation between CO₂/³He ratios and CO₂ concentrations. CO₂**
258 **concentrations are uniform in the spring samples, however CO₂/³He ratios are wide-ranging across the**
259 **typical mantle and crustal values. Vertical errors are smaller than symbols. Abbreviations of sample names**
260 **are given in Table 1.**

261 Neon, argon, krypton and xenon concentrations were measured in six CO₂ spring samples
262 (Taradale, Locarno, Deep Creek, Glenluce, Woolnoughs and Clifton Springs) (Table 2). ²⁰Ne/²²Ne
263 ratios of the spring samples range between 9.68 and 9.92, close the air value of 9.8 (Ballentine,
264 1997). ⁴⁰Ar/³⁶Ar ratios range from 299 to 314, slightly above the value of air (298.5) (Ozima and
265 Podosek, 2002). In contrast to relatively uniform and air-like isotope ratios, noble gas concentrations
266 are highly variable. ²⁰Ne concentrations vary over three orders of magnitude ($3.4 \pm 1.5 \times 10^{-8}$ to $1.4 \pm$
267 0.1×10^{-5}); ⁴⁰Ar concentrations vary from $5.3 \pm 0.2 \times 10^{-5}$ to $2.3 \pm 0.1 \times 10^{-4}$. Krypton and xenon
268 concentrations range from $8.3 \pm 0.3 \times 10^{-9}$ to $1 \pm 0.04 \times 10^{-8}$ and $6.9 \pm 0.4 \times 10^{-10}$ to $3.6 \pm 0.2 \times 10^{-9}$,
269 respectively.

270 4. Discussion – link between the CO₂ source in the reservoirs and 271 springs

272 4.1. He-CO₂ abundance system

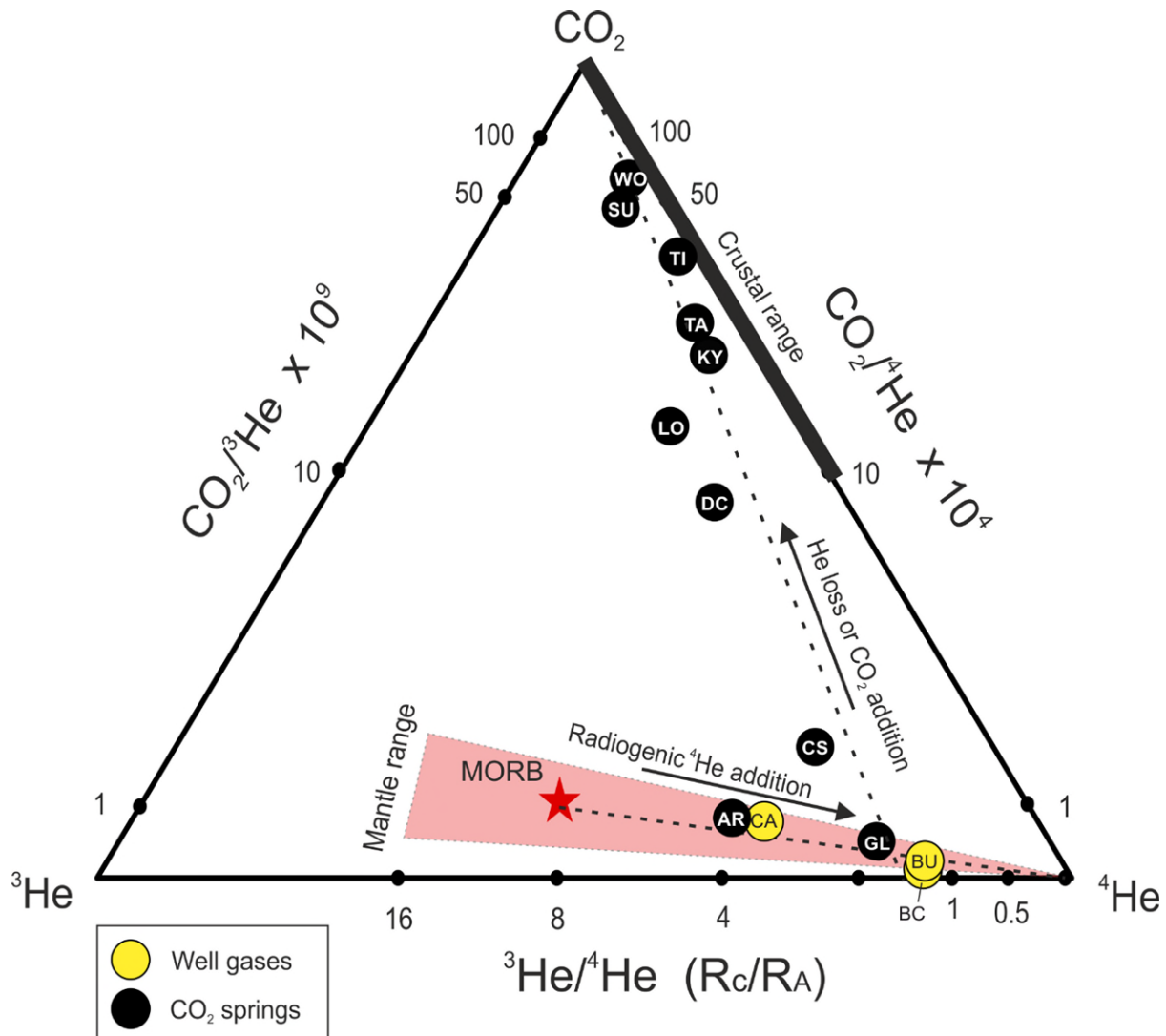
273 The trends in He-CO₂ abundance of well gases and CO₂ springs can be distinguished using a
274 ternary diagram after Giggenbach et al. (1993). This allows depiction of the relative ratios between
275 CO₂-³He-⁴He rather than absolute concentrations (Fig. 4). The MORB end-member (Marty and
276 Jambon, 1987) is displayed for reference with a straight mixing line showing addition of radiogenic
277 ⁴He. Caroline, Buttress, and Boggy Creek well gases as well as Argyle and Glenluce springs fall on a
278 mixing line between MORB and crustal end-members. The rest of the springs lie on the mixing
279 trajectory with low He/high CO₂ end-member (the CO₂ apex of the plot).

280 Based on the observed trends, two main processes can be identified. Addition of radiogenic
281 ⁴He to the MORB-type component lowers the ³He/⁴He, decreases CO₂/⁴He and does not affect
282 CO₂/³He ratio (the trend towards the ⁴He apex of the graph). All CO₂ well gas and spring samples
283 exhibit variation in ³He/⁴He ratios due to radiogenic ⁴He addition. Subsequently, either helium loss or
284 CO₂ addition increases both CO₂/³He and CO₂/⁴He but does not affect the ³He/⁴He ratios. The second

285 process affects the majority of the springs (excluding Glenluce and Argyle) but none of the well gas
286 samples (trajectory towards the CO₂ apex of the plot).

287 To evaluate this two-step process in the following discussion, we select two samples to use as
288 initial end-members. Argyle spring is representative of the regional high-mantle end member, least
289 affected by radiogenic ⁴He addition (exhibiting the highest measured ³He/⁴He ratio 3.65 of R_c/R_A,
290 [⁴He] = 8.8 ± 0.3 × 10⁻⁵ cm³(STP)/cm³). The highest He concentrations were measured in Glenluce
291 sample (³He/⁴He 1.57 R_c/R_A, [⁴He]=1.6 ± 0.1 × 10⁻⁴ cm³(STP)/cm³), which is the least affected by
292 secondary He loss or CO₂ addition.

293 The ³He/⁴He ratio can be modified by dilution with non-CO₂ gas (usually methane) with a
294 different He isotopic signature (Sherwood Lollar et al., 1994), radiogenic ⁴He accumulation in situ
295 (Newell et al., 2015; Liu et al., 2016) or He stripping from formation water during gas migration
296 through lithological units enriched in ⁴He (Sano et al., 1990; Sakamoto et al., 1992). The resulting
297 ³He/⁴He ratio can then be overprinted by addition of CO₂ from a different source (O'Nions and
298 Oxburgh, 1988) or phase fractionation during degassing (Matthews et al., 1987). If the well gases
299 and CO₂ springs share a common source, then these processes can be accounted for and gas
300 composition can be traced back to a single initial end-member.



301
 302 **Figure 4.** Ternary diagram (after Giggenbach et al., 1993) showing the relationship between the
 303 concentrations of CO₂, ³He, ⁴He expressed as their ratios. MORB value used for reference is 8 ± 1 R_A (Marty
 304 and Jambon, 1987). The dashed lines show mixing between different components. The two clear trends are:
 305 1) Radiogenic ⁴He addition, which shifts gas composition to the right apex of the ternary plot, 2) CO₂
 306 addition or He loss trend towards the top apex of the plot. Port Campbell well gases fall on the mixing line
 307 between MORB and crustal end-member. Spring samples fall on He loss/CO₂ addition trendline.
 308 Abbreviations of sample names are given in Table 1.

309 **4.2 Radiogenic ⁴He addition**

310 ⁴He is produced by the alpha decay of uranium and thorium in the crust. These elements are
 311 primarily concentrated in accessory minerals such as zircon and apatite, which release helium at a
 312 constant rate above the blocking temperature of the mineral (Tolstikhin et al., 2017). Similarly, ³He is
 313 produced by thermal neutron capture by ⁶Li, which can be approximated based on Li content of the
 314 crust (Ballentine and Burnard, 2002). However, this contribution is minimal relative to the amount of

315 ³He released from mantle fluids and can be considered to be negligible in the context of in-situ
316 crustal helium accumulation.

317 After production, radiogenic helium is either trapped in the pore spaces in-situ or mobilised by
318 any migrating water or gas phase present in the subsurface and then transported elsewhere. If a
319 natural gas trap exists in-situ, helium will preferentially accumulate in the gas phase due to its low
320 solubility in water.

321 4.2.1. Radiogenic ⁴He accumulation in-situ

322 The initial ³He/⁴He ratio of mantle-sourced gas can be reduced by direct accumulation of ⁴He
323 produced in the crust, or by mixing with ⁴He-rich methane. The former would be applicable to CO₂
324 springs, the latter to well gases containing CO₂ and CH₄ mixtures. In both cases, the final ⁴He
325 concentrations are controlled by the rate of ⁴He production in the crust. The contents of radiogenic
326 ⁴He accumulated in-situ in a natural gas trap can therefore be considered as a function of time since
327 the initial emplacement of the gas in the trap, given a known crustal helium production rate (Liu et
328 al., 2016). Under this assumption, we can estimate the residence time required for the observed
329 ³He/⁴He ratios in both the well gases and the springs.

330 The ⁴He production rate (Craig and Lupton, 1976) and ⁴He concentration in the pore fluid
331 increases at the rate of J_{He} (Torgersen, 1980):

$$332 \quad {}^4P = 0.2355 \times 10^{-12} \times [U] \times (1 + 0.123 \times [Th]/[U] - 4) \quad (1)$$

$$333 \quad J_{He} = {}^4P \times \rho \times (1 - \phi)/\phi \quad (2)$$

334 Where:

335 [U], [Th] – concentrations in ppm

336 ⁴P – crustal ⁴He production rate in cm³ STP g⁻¹ yr⁻¹

337 J_{He} – ⁴He production rate cm³(STP) yr⁻¹

338 ρ – density of the crust in g/cm³

339 φ – porosity of the rocks as a fraction

340 Assuming ⁴He has been accumulating in mantle-sourced CO₂ with a known initial composition,
341 the final ³He/⁴He ratio is expressed as a function of time (Newell et al., 2015):

342 ${}^3\text{He}/{}^4\text{He}(t) = F \times {}^3\text{He}_m / (J_{\text{He}} \times t + F \times {}^4\text{He}_m)$ (3)

343 Where:

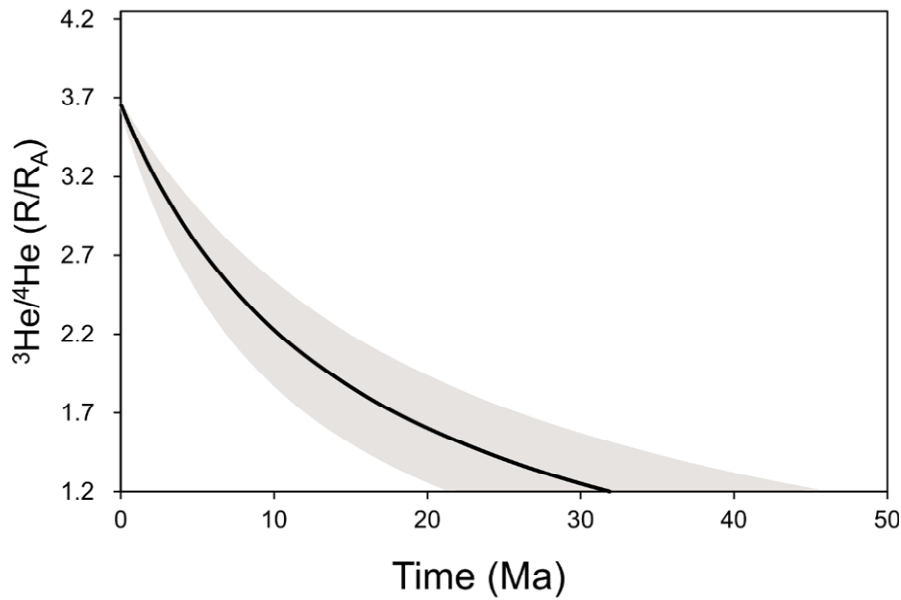
344 F – gas volume fraction in the rock

345 He_m – helium concentration of the mantle end-member

346 t – time in years

347 The final result is independent of the timing of CO₂ emplacement as it records the total ⁴He
348 accumulated since the start of the gas trap filling, so in the case of CO₂/methane mixture, the
349 recorded age will be that of the methane emplacement. Argyle spring concentrations are taken as
350 representative of the initial mantle end-member, based on the highest measured ³He/⁴He ratio.

351 Assuming an average reservoir porosity of 25 % (Watson et al., 2003), average crustal ²³⁸U and
352 ²³²Th concentrations of 2.8 and 10.7 ppm and assuming an average crustal density of 2.5 g/cm³
353 (Rudnick and Fountain, 1995) the estimated age of filling of the of Boggy Creek field is 32 Ma (Fig 5).
354 Assuming ± 5 % and ± 1 % uncertainty in porosity and ²³⁸U and ²³²Th concentrations respectively, the
355 accumulation age could vary between 22 and 45 Ma (showed in shaded area in Fig 5). This calculated
356 accumulation age range can be taken as a maximum, as the described method does not take into
357 account the contribution of helium stripped from water during the two stages of gas migration in the
358 reservoir and the initial ⁴He contents of the gas phase acquired from the source rock. Methane in
359 Port Campbell traps is associated with the last hydrocarbon generation stage that commenced
360 during the mid-Paleogene (Duddy, 1997; Boreham et al., 2004), which closely matches the range of
361 accumulation ages calculated. The ³He/⁴He ratios observed within the Boggy Creek and Buttress
362 fields can plausibly be explained by an Argyle-type mantle end-member mixing with thermogenic
363 methane containing radiogenic ⁴He, confirming the binary mixing with methane trend depicted in
364 Figure 4.



365

366 **Figure 5. $^3\text{He}/^4\text{He}$ ratio vs time since gas emplacement calculated for the composition of the Boggy Creek-1**
 367 **sample. To achieve the current $^3\text{He}/^4\text{He}$ ratio measured in Boggy Creek (1.21 R_A), Argyle-type CO_2 (3.65 R_A)**
 368 **would have to mix with methane that has been emplaced at 32 Ma. Shaded area shows uncertainty.**

369 The same calculation can be applied to the CO_2 springs. ^{238}U - ^{232}Th contents are assumed to be
 370 the same; the porosity of a fracture-dominated metasedimentary aquifer is estimated to be lower
 371 ($10 \pm 5\%$). To reduce the initial $^3\text{He}/^4\text{He}$ ratios of 3.65 to the lowest measured value of 1.23 R_A , it
 372 would take 9 Ma years on average and between 4-15 Ma within the uncertainty of the parameters.
 373 To account for the range of observed $^3\text{He}/^4\text{He}$ ratios, this scenario requires emplacement of separate
 374 gas pockets for each individual spring at different times between 9 Ma and present and retention
 375 within the crust before the onset of the recent migration to the surface.

376 Multiple gas injection events could be associated with discrete episodes of seismic or volcanic
 377 activity, although the latter is unlikely because the volcanic cones are far fewer than the individual
 378 mineral springs (>100) (Shugg, 2009), and given the predominately monogenetic eruptive character
 379 of the NVP extrusives (Boyce, 2013) volcanic activity is unlikely to produce so many different gas
 380 pulses. Irrespective of the gas emplacement mechanism, the heavily folded and fractured Ordovician
 381 metasedimentary sequence is unlikely to act as an effective gas trap for millions of years. In-situ ^4He
 382 accumulation in CO_2 springs is therefore an unlikely process to account for the observed variation in
 383 $^3\text{He}/^4\text{He}$ ratios.

384 4.2.2. Radiogenic ^4He stripping from enriched pore-water

385 An alternative model to in-situ generation is modification of magmatic $^3\text{He}/^4\text{He}$ ratios by
 386 dilution of mantle He during lateral movement of the CO_2 by radiogenic ^4He stripping from formation

387 water. This is a different process to interaction with ASW, which has already been accounted for
388 using He/Ne ratios to correct $^3\text{He}/^4\text{He}$ values for contribution of the atmospheric component
389 sourced from the formation water (Fig. 2). Instead, the stripping model considers radiogenic helium
390 accumulated and contained in the pore water of U/Th-enriched rocks. In this case the process is still
391 governed by the helium production rate in the crust (similar to the in-situ ^4He accumulation
392 discussed above), but the controlling factor is distance rather than time.

393 Assuming that mantle fluids are supplied through a single conduit at a constant rate under
394 steady-state homogenous and isotropic conditions under an equal hydrostatic pressure, the
395 variation in $^3\text{He}/^4\text{He}$ values can be accounted for by a hydrodynamic dispersion model (Sano et al.,
396 1990). $^3\text{He}/^4\text{He}$ is calculated as a function of the radial distance to the conduit (r) following the
397 approach detailed in Sano et al. (1990) of deriving the location-specific helium dispersion constant
398 (α) by fitting a least squares function to the measured $^3\text{He}/^4\text{He}$ and radial distance data points.

$$399 \quad ^3\text{He}/^4\text{He}(r) = ({}^3Pr^2 + \alpha {}^3\text{He}_m) / ({}^4Pr^2 + \alpha {}^4\text{He}_m) \quad (4)$$

400 Where:

401 r – radial distance from the main gas conduit

402 α – helium dispersion constant, dependent on the pore network geometry

403 P – crustal helium production rate in atoms/cm³s, calculated under the same crustal density and U,
404 Th content assumptions as in the ^4He accumulation model.

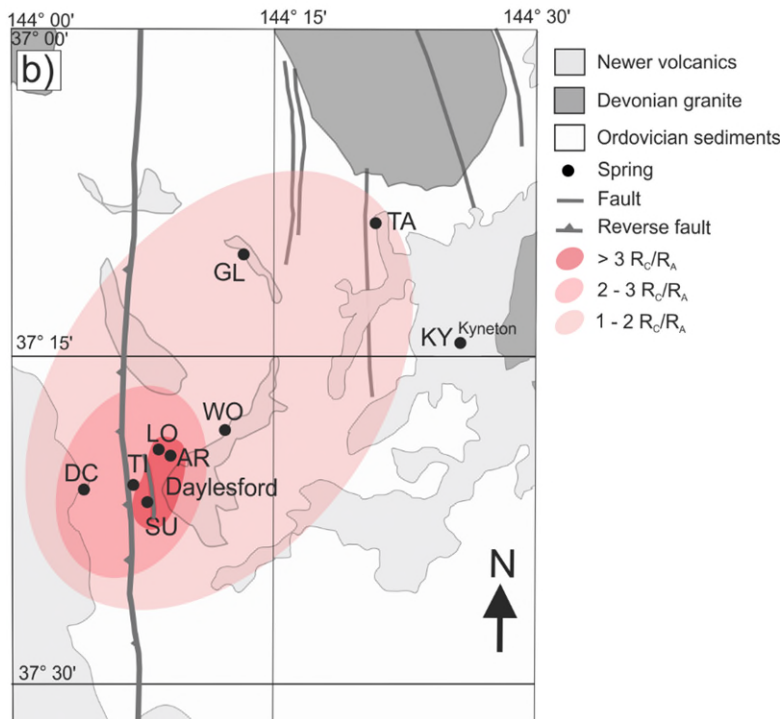
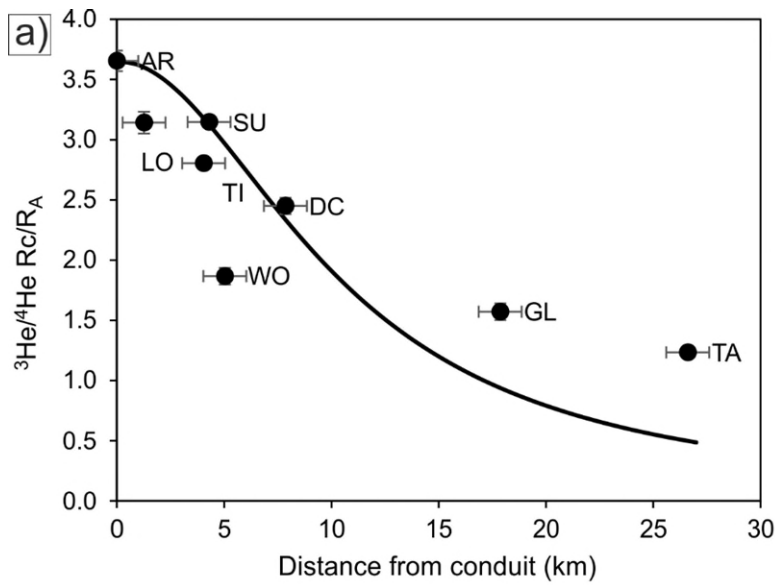
405 The Argyle spring (highest measured $^3\text{He}/^4\text{He}$ ratio of 3.65 R_A) is taken to be the closest to the
406 main conduit of mantle degassing in the CVH. Figure 6a shows the relationship between the $^3\text{He}/^4\text{He}$
407 ratios and the radial distance of sample location to the Argyle spring. Kyneton spring is excluded
408 from this because of its contamination with an atmospheric component. Samples with higher
409 $^3\text{He}/^4\text{He}$ ratios are located geographically closer to each other and the Argyle spring (Fig. 6b). Hence,
410 we propose that mantle CO₂ is being progressively diluted with a crustal component with increasing
411 distance from the inferred conduit.

412 The majority of the CO₂ migration prior to the degassing point occurs within the subsurface,
413 through ^4He -enriched basement rocks. The interaction with shallow ASW water occurs only at the
414 final stages of migration during the ascent to the surface, which explains the relatively high $^4\text{He}/^{20}\text{Ne}$
415 ratios and low atmospheric ^{20}Ne content in the majority of the samples. Similar decreases in $^3\text{He}/^4\text{He}$
416 ratios with increasing distance from a central volcanic cone has been observed in various active

417 volcanoes (Marty and Jambon, 1987; Williams et al., 1987; Sano et al., 1990; Sakamoto et al., 1992).
418 The $^3\text{He}/^4\text{He}$ distribution pattern is location-specific and controlled by the differences in the
419 topographic profile and the tortuosity of the fracture network, represented as constant α in
420 Equation 4.

421 The overall average rate of $^3\text{He}/^4\text{He}$ decrease in 4 volcanic locations reviewed by Sakamoto et
422 al. (1992) varied between 0.3 to 0.5 R_A/km . The average rate of $^3\text{He}/^4\text{He}$ decrease in CVH is 0.1
423 R_A/km , potentially reflecting fluid migration via more efficient fracture networks and conduits in a
424 faulted sequence relative to the previously investigated volcanic and volcanoclastic sequences.
425 Fractured aquifers have lower tortuosity relative to porous ones, which results in shorter effective
426 travel distance for the same total flow path distance (Clennell, 1997) and therefore lower rate of
427 radiogenic noble gas stripping per distance travelled.

428 Springs with the highest $^3\text{He}/^4\text{He}$ ratios are clustered near the N-S trending Muckleford Fault
429 and a smaller parallel fault striking along Lake Daylesford (Fig 6b). The spatial distribution of $^3\text{He}/^4\text{He}$
430 ratios controlled by helium dispersion along the flow pathways from the main conduit suggests that
431 one of these basement lineaments could be acting as a conduit through which mantle CO_2 is being
432 charged from depth. Previous studies have shown that clusters of NVP volcanic vents are commonly
433 aligned parallel to nearby basement faults throughout the province (van Otterloo et al., 2013; Cas et
434 al., 2017). Mantle xenoliths were found in the vicinity of the faults, suggesting fast mantle upwelling
435 rates through the lithosphere were prevalent during periods of magmatic activity (van Otterloo et
436 al., 2014). While further work is required to provide geomechanical and structural geological
437 evidence for current fluid migration along the fault zones in the CVH, these structures can
438 potentially play an important role in the currently active mantle- CO_2 ascent to the surface.



439

440 **Figure 6 a).** Plot of $^3\text{He}/^4\text{He } R_c/R_A$ values relative to the distance from the main conduit (measured on
 441 **Google Earth)** taking the highest $^3\text{He}/^4\text{He}$ ratio of Argyle spring as a starting value. The solid line is $^3\text{He}/^4\text{He}$
 442 **dispersion with distance model calculated based on (Sano et al., 1990).** **b).** Geographical distribution of CO_2
 443 **springs.** Springs with the highest $^3\text{He}/^4\text{He}$ ratios are clustered close to N-S trending basement-scale
 444 **Muckelford thrust fault and parallel smaller fault near Lake Daylesford.** Shaded areas show $^3\text{He}/^4\text{He}$ ratio
 445 **ranges which decrease with increasing distance from the Argyle spring.** Kyneton spring is excluded due to
 446 **atmospheric contamination.** Abbreviations of sample names are given in Table 1

447

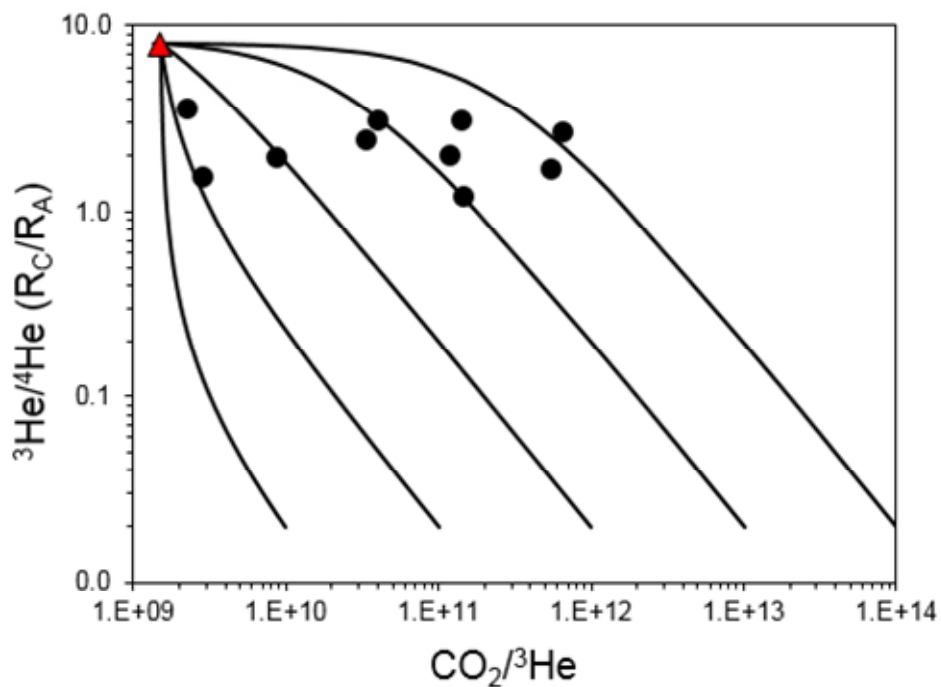
448 4.3. Evaluating models to account for CO₂/³He variation

449 The combination of CO₂ and helium is often used to identify the presence of mantle volatiles.
450 This is because CO₂/³He ratios have been well constrained for mantle-derived melts, fluids and
451 volatiles, with an average MORB value accepted as $1.5 \pm 0.5 \times 10^9$ (Sano and Marty, 1995; Marty and
452 Tolstikhin, 1998). ³He is not produced in significant amounts in the crust, so low ³He ratios and
453 associated CO₂/³He ratios between $10^{10} - 10^{15}$ are typically associated with a crustal CO₂ source
454 (O’Nions and Oxburgh, 1988). A trend in increasing CO₂/³He ratios is therefore often associated with
455 admixture of crustal CO₂ (e.g. Crossey et al., 2009; Newell et al., 2015; Ruzié et al., 2013). The
456 CO₂/³He ratios observed in ten CO₂ samples from the Victorian mineral springs vary over two orders
457 of magnitude (2.8×10^9 to 6.5×10^{11}), encompassing the range typical of mantle and crust end-
458 members.

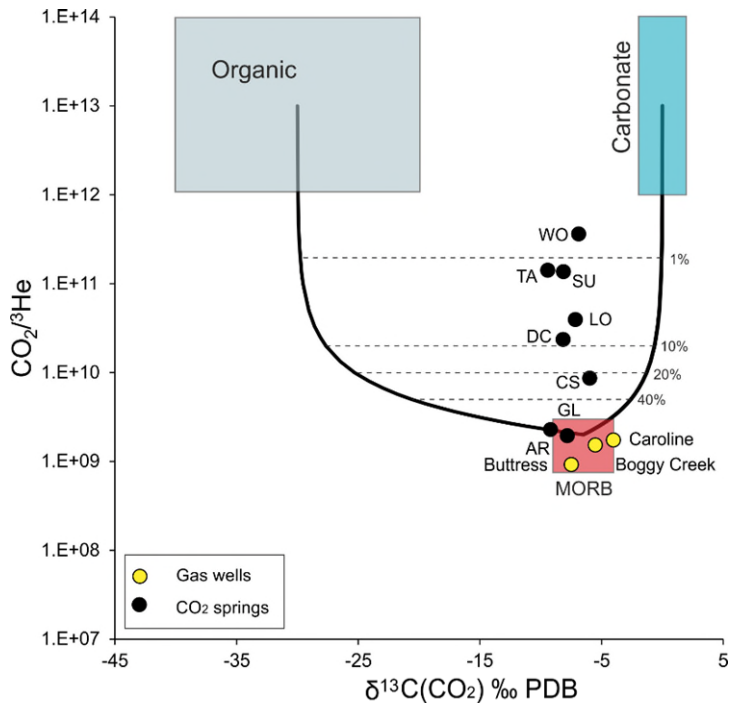
459 Crustal end-members can have a wide range of CO₂/³He ratios but a narrow range of ³He/⁴He
460 ratios (0.01 – 0.07) (Ozima and Podosek, 2002). Figure 7 shows CO₂/³He values plotted against
461 ³He/⁴He R_c/R_A ratios with binary mixing curves representing mantle (8 R_A) source and various crustal
462 components. Significantly, samples with high CO₂/³He ratios do not necessarily show lower ³He/⁴He
463 ratios, as would be expected in the case of mixing with ³He-poor crustal CO₂ source and trend
464 perpendicular to the calculated mixing lines. To explain the range of measured CO₂/³He ratios,
465 variable amounts of mixing with a wide range of different crustal reservoirs (CO₂/³He – $10^{10} - 10^{14}$)
466 would need to be invoked, which is unlikely in the setting where bedrock geology is uniform across
467 the area.

468 Crustal CO₂ addition can be further assessed by combining He data with δ¹³C(CO₂) values
469 (Sano and Marty, 1995). The range of δ¹³C(CO₂) values measured in the springs (-9.4 to -6‰) are
470 outside the typical mantle (-7 to -4‰) range (Wycherley et al., 1999). However, increasing CO₂/³He
471 ratios do not consistently correlate with δ¹³C(CO₂) change towards carbonate or organic end-
472 members (Fig. 8). Instead, a vertical trend exists, which would require mixing with an end-member
473 with constant proportions of both organic and carbonate-sourced CO₂. To explain the highest
474 observed CO₂/³He ratios, 99 % of non-mantle (crustal/organic mixture) CO₂ addition is required. Such
475 significant amounts of crustal CO₂ sourced by dissolution of bedrock minerals would liberate cations
476 contained in the dissolving minerals and increase the TDS values of the water. Figure 9 shows that
477 there is no clear positive correlation between the CO₂/³He ratios in the volatiles and TDS values in
478 their associated waters.

479 Previous geochemical modelling work showed that CO₂ does not cause significant amounts of
 480 bedrock mineral dissolution in the Ordovician aquifer (Karolytè et al., 2017) and there is no
 481 geological evidence for addition of large amounts of crustal CO₂ from other sources (e.g. carbonate
 482 metamorphism). The possibility of significant amounts of organic CO₂ addition is also ruled out,
 483 because the observed trend on Figure 8 cannot be explained by addition of organic CO₂ in the
 484 absence of the crustal component. Based on the combined evidence from $\delta^{13}\text{C}(\text{CO}_2)\text{-He}$, CO₂
 485 abundance and TDS contents of the mineral waters, we conclude that there is no significant crustal
 486 CO₂ addition to the mantle volatiles sampled at the CVH and Clifton Springs.

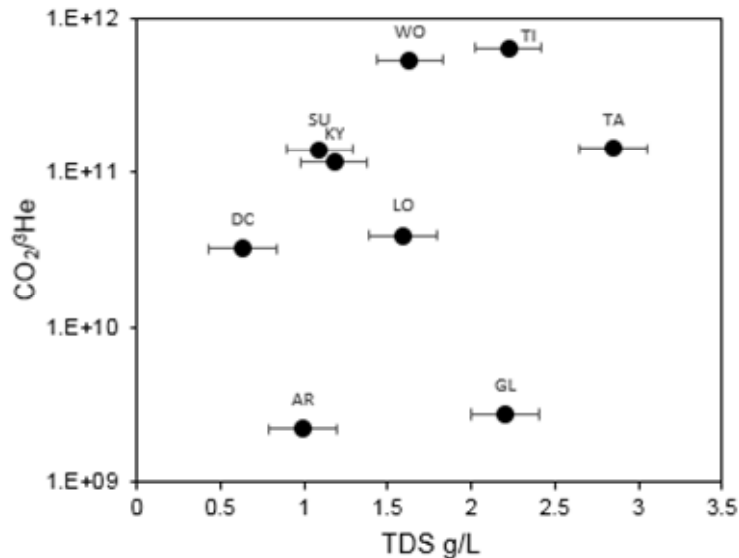


487
 488 **Figure 7. Binary mixing plot between MORB (red triangle) ($^3\text{He}/^4\text{He}$ 8 R_A , $\text{CO}_2/^3\text{He}$ 1.5×10^9) and various**
 489 **crustal end-members ($\text{CO}_2/^3\text{He}$ $10^{10}\text{-}10^{14}$). The springs form a near-horizontal trendline and do not follow**
 490 **any of the mixing lines, suggesting that mixing does not control the variation in $\text{CO}_2/^3\text{He}$ values. All error**
 491 **bars are smaller than the printed symbols.**



492

493 **Figure 8. $\text{CO}_2/{}^3\text{He}$ ratios vs $\delta^{13}\text{C}$ values for gas samples in relation to mixing between the mantle, carbonate**
 494 **and organic CO_2 end-members based on Sano and Marty, 1995. Caroline, Boggy Creek and Buttress well**
 495 **gases fall within the mantle range. Spring samples do not show a coherent trend towards either an organic**
 496 **or carbonate CO_2 end member. The observed trend would require > 99% contribution of a component with**
 497 **constant proportions of both organic and carbonate-sourced CO_2 ; however, this is not supported by other**
 498 **data (discussed in text). Abbreviations of sample names are given in Table 1.**



499

500 **Figure 9. CO₂/³He vs TDS measured in borehole water sampled via hand pumps. CO₂/³He values are not**
 501 **correlated with TDS. A positive correlation would be expected if crustal CO₂ was added as a result of**
 502 **bedrock mineral dissolution.**

503 Alternatively to mixing with different CO₂ sources, the variability of δ¹³C(CO₂) values (-9.4 to -
 504 6‰) can be explained by degassing under a range of different pH and temperature conditions.
 505 Equilibrium fractionation between δ¹³C(CO₂) in aqueous and gaseous phases is controlled by the
 506 temperature and the relative amounts of HCO₃⁻ and H₂CO₃, which are pH-dependent. If H₂CO₃ is the
 507 dominant DIC species, degassing CO₂ is slightly enriched in ¹³C. Conversely, when HCO₃⁻ dominates
 508 the system, degassing CO₂ is relatively depleted in ¹³C (Deines et al., 1974). The pH values measured
 509 in mineral water bores range from 5.5 to 6.1 and temperatures are 15 – 21 °C. In this particular
 510 range of conditions, the ratio of HCO₃⁻ to H₂CO₃ in DIC varies significantly. The resulting calculated
 511 equilibrium enrichment factors between DIC and gaseous CO₂ range from -3.4 to -0.43‰. Degassing
 512 under different DIC speciation conditions therefore can fully account for the observed 3.4‰
 513 variability in δ¹³C(CO₂) values of the spring gases.

514 4.4 Noble gas abundance modification by near-surface degassing

515 The variation observed in ³He concentrations in the mineral spring samples is also replicated
 516 in ⁴He and other noble gases. Importantly, the range in which concentrations vary decreases with
 517 element mass (Fig. 10). This suggests that the large differences in elemental abundance between the
 518 spring samples could be caused by a physical fractionation, post-dating the mixing of mantle and
 519 ASW sources. CO₂ springs are a dynamic two-phase system where equilibrium partitioning between
 520 water and gas during mineral water ascent to the surface is likely to occur.

521 Noble gas solubility in water increases with element mass. During equilibration in a two-phase
 522 water and gas system, noble gases are partitioned between gas and water according to their
 523 solubility coefficient, as defined by Henry's Law (Ballentine et al., 2002):

$$524 \quad C_{ig} = K_i \times C_{iw} \quad (5)$$

525 Where C is concentration, subscripts g and w denote gas and water phases and K_i is Henry's
 526 constant for noble gas i . K_i is temperature, pressure and salinity dependent (Kipfer et al., 2002). For
 527 the purpose of investigating a shallow degassing process, we assume equilibration with fresh water
 528 at atmospheric pressure and 20 °C temperature. Henry's constants and activity coefficients for water
 529 conditions were calculated from empirical equations from Crovetto et al. (1982) for Ne, Ar, Kr and Xe
 530 and Smith (1985) for He, following the methodology in Ballentine and Burnard (2002).

531 In a closed system, the total noble gas contents are conserved but redistributed between the
 532 two phases according to the relative gas/water volume ratios. In the situation where the initial
 533 concentration in the gas phase is known (C_{ig}^0), the associated equilibrium concentration in water
 534 (C_{iw}^0) can be calculated from Equation 5. Redistribution of the noble gas contents between the two
 535 phases can then be expressed as a function of volume, where $\frac{V_g}{V_t}$ is the fraction of the total volume
 536 occupied by gas and C_{ig}^f is the final concentration in the gas phase:

$$537 \quad C_{ig}^f = C_{ig}^0 \times \frac{V_g}{V_t} + C_{iw}^0 \times \left(1 - \frac{V_g}{V_t}\right) \quad (6)$$

538 The final noble gas concentrations measured in CO₂ degassing at the surface are a result of the
 539 initial dissolution in water and subsequent degassing, which can occur in two or more steps under
 540 different water/gas ratios. However, the final result is independent of these variations as long as the
 541 system remains closed. In reality, solubility constant K_i will differ slightly during dissolution and
 542 degassing steps depending on depth and temperature conditions, but the overall difference will be
 543 far smaller than that caused by the difference in gas/water volume ratios.

544 A scenario where $\frac{V_g}{V_t} = 1$ describes simple equilibrium partitioning at given pressure and
 545 temperature, in this case under atmospheric pressure at the surface, where there are no constraints
 546 other than atmospheric pressure to the volume of the gas phase. In this case $C_{ig}^f = C_{ig}^0$ and water
 547 noble gas contents are in accordance with atmospheric equilibrium. In the opposite case, when gas
 548 volume fraction ratio is becoming infinitesimally small ($\frac{V_g}{V_t} \rightarrow 0$), noble gas contents are dissolved in
 549 water and $C_{ig}^f \rightarrow C_{iw}^0$. The $\frac{V_g}{V_t} \rightarrow 0$ scenario describes a situation where constraints in space limit the

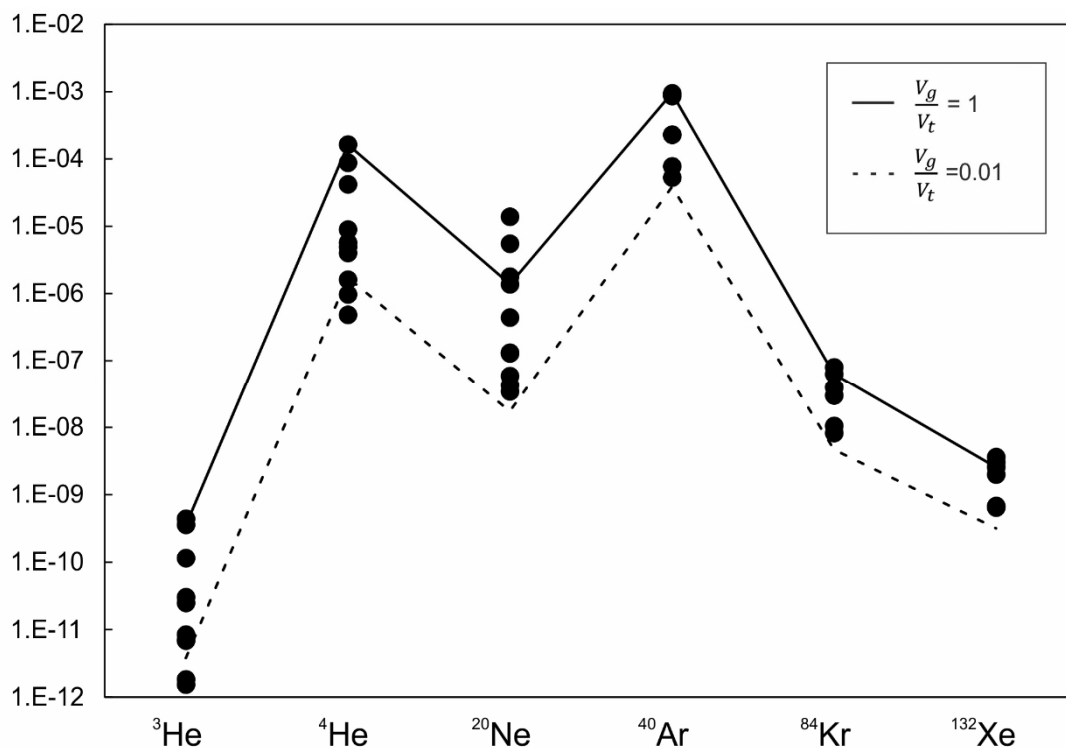
550 volume expansion and result in overpressure. Because volume ratios are expressed as a fraction of
551 the total volume, the possible values range from 0 to 1.

552 The wide range of noble gas concentrations in the CO₂ springs allows a test of whether
553 variations in $\frac{V_g}{V_t}$ ratios correlate with measured noble gas contents consistently across different
554 element pairs. The highest helium concentrations were measured in Glenluce spring, which is taken
555 to be representative of the least fractionated gas phase. We make an assumption that Glenluce
556 degassed under $\frac{V_g}{V_t} = 1$ conditions with no external gas stripping mechanism based on field
557 observations of intermittent bubble formation and an overall low CO₂ flux. Under these assumptions
558 C_{ig}^f can be calculated for different $\frac{V_g}{V_t}$ ratios. This approach does not require separate calculation of
559 noble gases degassing from ASW, as the final noble gas concentrations measured from each spring
560 are a sum of the total noble gas contents derived from the both water and the original mantle
561 sources.

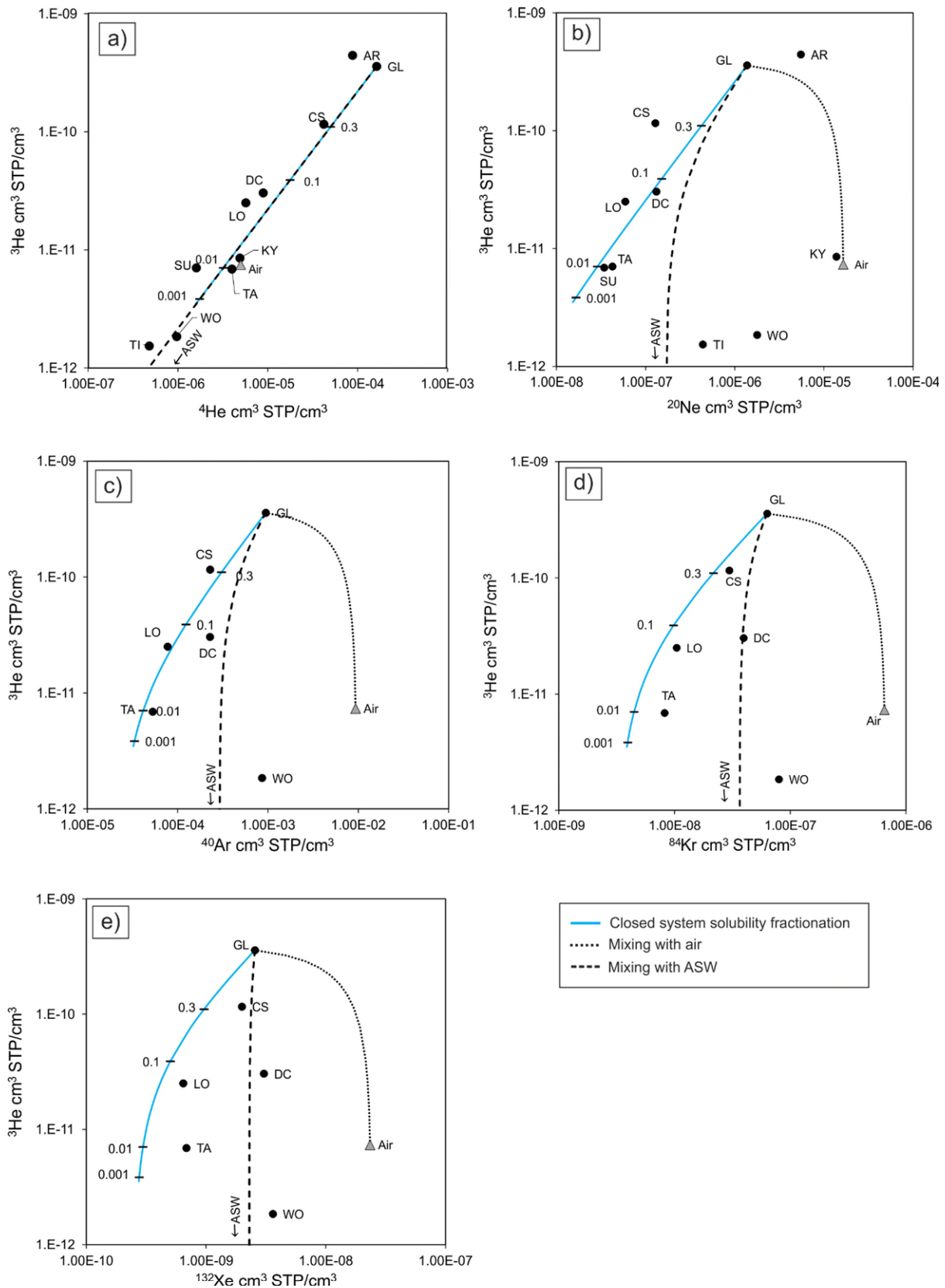
562 Figure 10 shows the distribution of noble gas concentrations in the studied springs. The range
563 in observed gas concentrations decreases with element mass. The solid black line shows
564 concentrations of $\frac{V_g}{V_t} = 1$ where no fractionation between elements occurs and the final
565 concentrations are the same. The dashed line shows $\frac{V_g}{V_t} = 0.01$ scenario where fractionation is close
566 to the maximum possible in a closed system and $C_{ig}^f \rightarrow C_{iw}^0$. All data points plot within the bounds
567 of these two end-member scenarios and can therefore be interpreted as fractionated within a closed
568 system. The progressive loss of noble gas concentrations correlates across all noble gas elemental
569 pairs.

570 Figure 11 shows ³He concentrations relative to ⁴He, ²⁰Ne, ⁴⁰Ar, ⁸⁴Kr and ¹³²Xe. Solid blue lines
571 show calculated fractionation trends from the initial composition of Glenluce, with black tick marks
572 showing the $\frac{V_g}{V_t}$ ratio. The noble gas concentrations follow a negative trend in all elemental pairs with
573 $\frac{V_g}{V_t}$ ranging from 0.3 (Clifton Springs) to 0.01 (Taradale and Sutton). Deviation from a closed system
574 scenario occurs if the system is partially open to gas or water loss and input. Gas can be added by
575 mixing with air, both gas and water can be added by admixture of ASW and finally gas can be
576 removed from the system prior to the point of sample collection. If gas is lost prior to sampling,
577 equation 6 no longer holds true and the final gas concentrations are not limited to those of the initial
578 water ($\frac{V_g}{V_t} \rightarrow 0$, $C_{ig}^f \rightarrow C_{iw}^0$ scenario). Alternatively, the initial gas concentration C_{ig}^0 could be
579 modified by mixing with ASW or air.

580 ^3He and ^4He values in Tipperary and Woolnoughs springs are lower than predicted by the
 581 closed system model, which can be explained by mixing with both ASW and water (Fig. 11). This is
 582 obvious in different element pair plots (Figs. 11 b,c,d,e) and less apparent in ^3He vs ^4He (Fig. 11a)
 583 because air and ASW have similar $^3\text{He}/^4\text{He}$ ratios. Figure 11b also clearly shows that solubility
 584 fractionation in Kyneton spring has been overprinted by admixture of air, most likely during sample
 585 collection and clearly identified in the $^4\text{He}/^{20}\text{Ne}$ ratios, as previously mentioned. Clifton Springs,
 586 Deep Creek, Locarno and Taradale samples plot between solubility fractionation and mixing with
 587 ASW lines in Figure 11 c,d,e illustrating the additions of a small component derived from ASW, the
 588 influence of which is more evident in the heavier atmospheric noble gases.



589
 590 **Figure 10. Noble gas concentrations of CO₂ spring samples in cm³ (STP)/cm³. The variation in concentrations**
 591 **decreases with relative noble gas mass. This is explained by partitioning between water and gas phases**
 592 **during degassing, assuming a closed system. Black solid and dashed lines show expected gas concentrations**
 593 **for final V_g/V_w ratios of 1 and 0.01, respectively. The data are in good agreement with the model indicating a**
 594 **closed system, with exceptions of depletion in He and enrichment in Ne in samples that have equilibrated**
 595 **with a mixture of ASW and air (discussed in text). The extent of fractionation for different noble gases**
 596 **decreases with increasing mass and is directly dependent on their relative solubilities in water.**
 597 **Abbreviations of sample names are given in Table 1.**



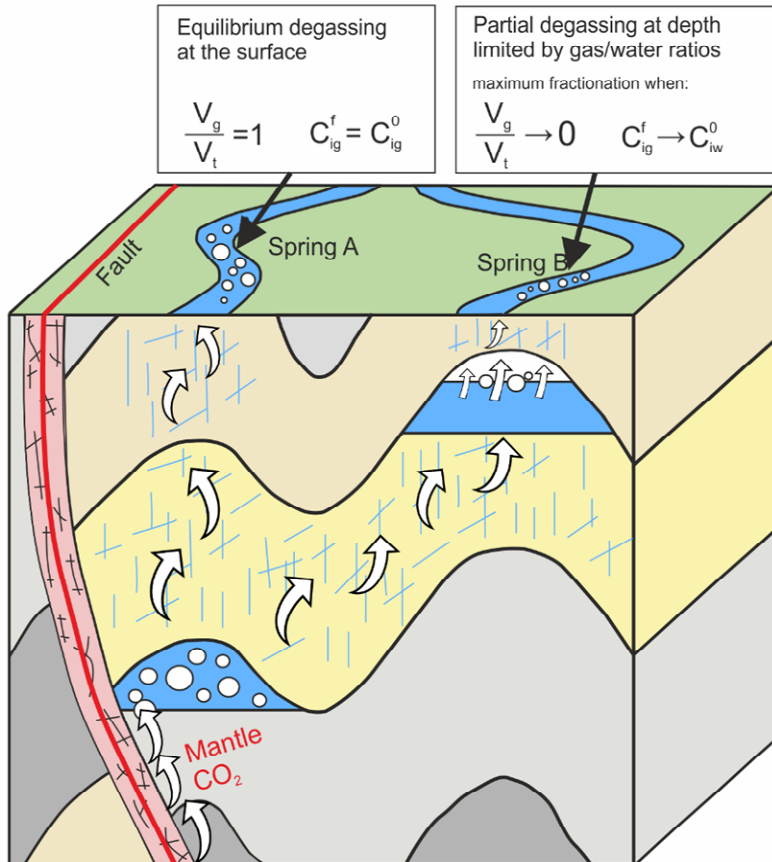
598

599 **Figure 11.** ^3He concentrations relative to ^4He (a), ^{20}Ne (b), ^{40}Ar (c), ^{84}Kr (d) and ^{132}Xe (e) in $\text{cm}^3(\text{STP})/\text{cm}^3$. Solid
 600 black lines show calculated concentrations assuming degassing from the initial Glenluce composition, with
 601 decreasing V_g/V_t ratio from 1 to 0.001, marked by black tick marks. Dashed lines show mixing with ASW at

602 20 °C; dotted line shows mixing with air. All samples can be explained by fractionation during degassing at
603 V_g/V_t ranging from 1 to 0.01 with some deviation from the calculated trendline due to mixing with ASW
604 and/or air. a) All samples fall within the calculated line except for TI and WO springs. b) shows that this is
605 because TI and WO have a contribution between ASW and air components, plotting between these end-
606 members. This is consistently replicated for Woolnoughs spring in c) d) and e). Ar, Kr and Xe concentrations
607 of CS, DC, LO and TA springs are within the limits of mixing with ASW and calculated degassing fractionation
608 line. Abbreviations of sample names are given in Table 1.

609 The conceptual model of CO₂ migration to the surface is summarised in Figure 12. The initial
610 mixing between mantle and ASW noble gas components occurs when mantle CO₂ migrates and
611 dissolves in groundwater. The mineral water with dissolved noble gas contents ascends to the
612 surface via individual restricted fracture corridors and manifests at the surface as separate
613 geographically dispersed springs. The nucleation of the gas phase in water occurs when partial
614 pressures of dissolved gases exceed the hydrostatic pressure. Partial pressures of noble gases are
615 too low to trigger the degassing at depth, so the process is controlled by the CO₂ saturation level of
616 the water. Once the dominating gas phase (CO₂) is oversaturated and begins degassing, the other
617 dissolved gas species will partition between the two phases based on gas/water volumetric ratio.

618 After equilibrium separation water and CO₂ migrate to the surface as a two-phase flow and do
619 not re-equilibrate again. This implies that in instances where degassing occurs at depth, sampled
620 gases are expected to contain lower concentrations of noble gases because of the limiting effect of
621 gas volume being restricted to that of CO₂. In contrast, mineral waters with lower CO₂ partial
622 pressures nucleate into the gas phase at surface equilibrium conditions and therefore contain higher
623 overall noble gas contents. This finding suggests that noble gas tracing of shallow leakage is more
624 sensitive and the original composition is better preserved where overall CO₂ partial pressures are
625 lower and degassing occurs at or very near to the surface. Noble gases are therefore particularly
626 sensitive tracers to small scale gas migration and should be considered for surface monitoring of any
627 industrial site where fugitive gas emission is a possibility.



628

629 **Figure 12. Schematic cartoon of CO₂ and mineral water migration. Mantle CO₂ ascends through a fault zone**
 630 **and dissolves in groundwater. Water charged with CO₂ migrates through a fractured aquifer to the surface.**
 631 **In spring A, with a low gas flux, gas/water separation occurs at the surface under equilibrium conditions and**
 632 **the final degassed gas phase retains its original concentrations. In the case of spring B, with a higher gas flux,**
 633 **gas/water separation occurs at depth when CO₂ becomes oversaturated in water. Noble gases partition**
 634 **between water and gas phases under the same equilibrium conditions, but the partitioning is limited by the**
 635 **gas volume.**

636 5. Conclusions

637 $^3\text{He}/^4\text{He}$ and $\text{CO}_2/^3\text{He}$ ratios in well gas and CO_2 spring samples in the Otway Basin and the
638 Central Victorian Highlands show unambiguous evidence for a predominantly mantle origin for the
639 CO_2 stored in the gas fields and actively migrating to the surface at the springs. The main processes
640 modifying noble gas geochemical signatures are crustal ^4He addition and noble gas fractionation
641 between the water and gas phases during degassing. $^3\text{He}/^4\text{He}$ ratios in well gases vary due to mixing
642 with methane, which has crustal helium contents directly dependent on gas residence time in the
643 reservoir.

644 The $^3\text{He}/^4\text{He}$ ratio variation in CO_2 springs is controlled by hydrodynamic dispersion and is
645 directly dependent on the radial distance to the gas supply conduit. The observed decline in $^3\text{He}/^4\text{He}$
646 ratios with distance suggests that CO_2 is supplied from a single conduit in the area around Argyle
647 spring. $^3\text{He}/^4\text{He}$ ratios are the highest in samples clustered near the Muckleford Fault and smaller
648 parallel faults in its vicinity, suggesting that one of these basement lineaments could be acting as a
649 pathway for mantle CO_2 to reach the shallow subsurface.

650 The variability of noble gas abundance patterns observed in the CO_2 springs can be explained
651 by closed system solubility fractionation during degassing. The gas to water ratio at the time of
652 phase separation controls the distribution of noble gases between the water and gas phases. The
653 original noble gas composition of CO_2 springs is uniform and only altered by near-surface degassing
654 during the final stages of CO_2 ascent to the surface, dependent on CO_2 flux; the $\delta^{13}\text{C}(\text{CO}_2)$ values are
655 controlled by degassing at pH range of 5.8 - 6.3. Original noble gas signatures are better preserved in
656 samples where overall CO_2 partial pressures are lower and degassing occurs at or very near the
657 surface.

658 Taking these processes into account, noble gas compositions observed in well gases in Port
659 Campbell, Mount Gambier, as well as CO_2 springs in CVH and Clifton Springs are traced back to a
660 single end member of $^3\text{He}/^4\text{He}$ of 3.07 - 3.65 R_A , proving a common source. This implies a uniform
661 regional gas composition in the Otway basin and CVH.

662 Importantly, we present evidence that ^3He loss resulting in high $\text{CO}_2/^3\text{He}$ ratios, commonly
663 associated with crustal CO_2 addition, can be explained without the need to invoke mixing with
664 crustal CO_2 , which is especially important in the absence of a clear mixing trend in $\delta^{13}\text{C}(\text{CO}_2)$ values.
665 Hence, $\text{CO}_2/^3\text{He}$ values should be compared to the concentrations of other noble gases and used
666 with caution when assessing the origin of CO_2 degassing at surface springs.

667 The techniques outlined in this paper can be used to identify the origin of CO₂ seeps at the
668 surface and their connectivity to reservoir gases. Hence, they can be applied to CO₂ sequestration or
669 other industrial fugitive gas monitoring settings, such as surrounding shale gas operations. Helium-
670 CO₂ abundance relationship can be used to determine the gas connectivity as long as the industrial
671 gas has a different initial He isotope ratio to the ASW end-member. The genetic link between
672 separate CO₂ seeps can be tested by applying solubility fractionation modelling to account for
673 changes in noble gas concentrations caused by near-surface degassing.

674 Noble gas signatures have been observed to be better preserved in cases where CO₂
675 saturation levels in water are low and degassing occurs near or at the surface. This means that noble
676 gases are therefore particularly sensitive tracers to small-scale gas migration and should be
677 considered for surface monitoring of any industrial site where emission of fugitive gas is possible.

678 Acknowledgments

679 This work was supported by an EPSRC PhD studentship in partnership with CO₂CRC and
680 Badley Geoscience Ltd. G. Johnson and S. Gilfillan were partially supported by both UKCCSRC and
681 Scottish Carbon Capture and Storage (SCCS), S. Serno was funded by the UK Carbon Capture and
682 Storage Research Centre (UKCCSRC) Call 2 grant. S. Flude was supported by by EPSRC grant
683 #EP/K036033/1. We thank the field operators – BOC, Air Liquide and CO₂CRC for permission to
684 sample the gas reservoirs. Craig Vivian and Peter Dumsey are thanked for support while sampling in
685 the field. We thank Terry Donnelly and Marta Zurakowska at SUERC for assistance in obtaining stable
686 isotope and noble gas measurements of gas samples. Ian Cartwright is thanked for providing
687 background data on the Daylesford springs.

688 References

- 689 Aeschbach-Hertig W., El-Gamal H., Wieser M. and Palcsu L. (2008) Modeling excess air and degassing
690 in groundwater by equilibrium partitioning with a gas phase. *Water Resour. Res.* **44**, 1–12.
- 691 Aka F. T., Kusakabe M., Nagao K. and Tanyileke G. (2001) Noble gas isotopic compositions and
692 water/gas chemistry of soda springs from the islands of Bioko, São Tomé and Annobon, along
693 with Cameroon Volcanic Line, West Africa. *Appl. Geochemistry* **16**, 323–338.
- 694 Akbari V. (1992) *Boggy Creek No.1 Well Completion Report.*, Available at: [http://geoscience-web.s3-
695 website-ap-southeast-2.amazonaws.com/well/boggycreek1.htm](http://geoscience-web.s3-website-ap-southeast-2.amazonaws.com/well/boggycreek1.htm).
- 696 Baines S. J. and Worden R. H. (2004) The long term fate of CO₂ in the subsurface: natural analogues
697 for CO₂ storage. In *Geological Storage of Carbon Dioxide* (ed. R. H. Baines, S.J., Worden).
698 Geological Society, London. pp. 59–85.
- 699 Ballentine C. J. (1997) Resolving the mantle He/Ne and crustal ²¹Ne/²²Ne in well gases. *Earth
700 Planet. Sci. Lett.* **152**, 233–249.
- 701 Ballentine C. J., Burgess R. and Marty B. (2002) Tracing Fluid Origin, Transport and Interaction in the
702 Crust. *Rev. Mineral. Geochemistry* **47**, 539–614.
- 703 Ballentine C. J. and O’Nions R. K. (1994) The use of natural He, Ne and Ar isotopes to study
704 hydrocarbon-related fluid provenance, migration and mass balance in sedimentary basins.
705 *Geol. Soc. London, Spec. Publ.* **78**, 347–361.
- 706 Ballentine C. J., O’Nions R. K. and Coleman M. L. (1996) A Magnus opus: Helium, neon, and argon
707 isotopes in a North Sea oilfield. *Geochim. Cosmochim. Acta* **60**, 831–848.
- 708 Barry P. H., Lawson M., Meurer W. P., Warr O., Mabry J. C., Byrne D. J. and Ballentine C. J. (2016)
709 Noble gases solubility models of hydrocarbon charge mechanism in the Sleipner Vest gas field.
710 *Geochim. Cosmochim. Acta* **194**, 291–309.
- 711 Bernecker T. and Moore D. H. H. (2003) Linking basement and basin fill: implications for hydrocarbon
712 prospectivity in the Otway Basin Region. *APPEA J.* **43**, 39–58.
- 713 Boreham C. J., Hope J. M., Jackson P., Davenport R., Earl K. L., Edwards D. S., Logan G. A. and Krassay
714 A. A. (2004) Gas – oil – source correlations in the Otway Basin, southern Australia. In *Petroleum
715 Exploration Society of Australia (PESA)*. pp. 19–22.

- 716 Boreham C., Underschultz J., Stalker L., Kirste D., Freifeld B., Jenkins C. and Ennis-King J. (2011)
 717 Monitoring of CO₂ storage in a depleted natural gas reservoir: Gas geochemistry from the
 718 CO₂CRC Otway Project, Australia. *Int. J. Greenh. Gas Control* **5**, 1039–1054.
- 719 Bosch A. and Mazor E. (1988) Natural gas association with water and oil as depicted by atmospheric
 720 noble gases: case studies from the southeastern Mediterranean Coastal Plain. *Earth Planet. Sci.*
 721 *Lett.* **87**, 338–346.
- 722 Boulton P. J., Johns D. R. and Lang S. C. (2004) Subsurface plumbing of the Crayfish Group in the Penola
 723 Trough: Otway Basin. In *Eastern Australasian Basins Symposium II Petroleum Exploration*
 724 Society of Australia (PESA). pp. 483–498.
- 725 Boyce J. (2013) The Newer Volcanics Province of southeastern Australia: a new classification scheme
 726 and distribution map for eruption centres. *Aust. J. Earth Sci.* **60**, 449–462.
- 727 Caffee M. W. (1999) Primordial noble gases from Earth's mantle: identification of a primitive volatile
 728 component. *Science (80-)*. **285**, 2115–2118.
- 729 Cartwright I., Weaver T., Tweed S., Ahearne D., Cooper M., Czapnik K. and Tranter J. (2002) Stable
 730 isotope geochemistry of cold CO₂-bearing mineral spring waters, Daylesford, Victoria,
 731 Australia: Sources of gas and water and links with waning volcanism. *Chem. Geol.* **185**, 71–91.
- 732 Cas R. A. F., van Otterloo J., Blaikie T. N. and van den Hove J. (2017) The dynamics of a very large
 733 intra-plate continental basaltic volcanic province, the Newer Volcanics Province, SE Australia,
 734 and implications for other provinces. *Geol. Soc. London, Spec. Publ.* **446**, 123–172.
- 735 Cayley R. A., Korsch R. J., Moore D. H., Costelloe R. D., Nakamura A., Willman C. E., Rawling T. J.,
 736 Morand V. J., Skladzien P. B. and O'Shea P. J. (2011) Crustal architecture of central Victoria:
 737 Results from the 2006 deep crustal reflection seismic survey. *Aust. J. Earth Sci.* **58**, 113–156.
- 738 Chivas A. R. ., Barnes I. E. ., Lupton J. E. . and Collerson K. (1983) Isotopic studies of south-east
 739 Australian CO₂ discharges. *Geol. Soc. Aust. Abstr.* **12**, 94–95.
- 740 Chivas A. R., Barnes I., Evans W. C., Lupton J. E. and Stone J. O. (1987) Liquid carbon dioxide of
 741 magmatic origin and its role in volcanic eruptions. *Nature* **326**, 587–589.
- 742 Clennell M. Ben (1997) Tortuosity: a guide through the maze. *Geol. Soc. London, Spec. Publ.* **122**,
 743 299–344.
- 744 Coulson A. (1933) The older volcanic and Tertiary marine beds at Curlewis, near Geelong. *Proc. R.*

- 745 *Soc. Victoria* **45**, 140–149.
- 746 Cox S. F., Sun S. S., Etheridge M. A., Wall V. J. and Potter T. F. (1995) Structural and geochemical
747 controls on the development of turbidite- hosted gold quartz vein deposits, Wattle Gully mine,
748 central Victoria, Australia. *Econ. Geol.* **90**, 1722–1746.
- 749 Craig H. (1978) A mantle helium component in circum-Pacific volcanic gases: Hakone, the Marianas
750 and Mt. Lassen. *Terrestrial Rare Gases*, 3–16.
- 751 Craig H. and Lupton J. E. (1976) Primordial neon, helium, and hydrogen in oceanic basalts. *Earth*
752 *Planet. Sci. Lett.* **31**, 369–385.
- 753 Crossey L. J., Karlstrom K. E., Springer A. E., Newell D., Hilton D. R. and Fischer T. (2009) Degassing of
754 mantle-derived CO₂ and He from springs in the southern Colorado Plateau region - Neotectonic
755 connections and implications for groundwater systems. *Bull. Geol. Soc. Am.* **121**, 1034–1053.
- 756 Crovetto R., Fernández-Prini R. and Japas M. L. (1982) Solubilities of inert gases and methane in H₂O
757 and in D₂O in the temperature range of 300 to 600 K. *J. Chem. Phys.* **76**, 1077–1086.
- 758 Dahlhaus (2003) *The Dell, Clifton Springs. 3-dimensional geological model.*, Available at:
759 [http://www.ccmaknowledgebase.vic.gov.au/soilhealth/soils_resource_details.php?resource_id](http://www.ccmaknowledgebase.vic.gov.au/soilhealth/soils_resource_details.php?resource_id=2416)
760 [=2416](http://www.ccmaknowledgebase.vic.gov.au/soilhealth/soils_resource_details.php?resource_id=2416).
- 761 Darrah T. H., Vengosh A., Jackson R. B., Warner N. R. and Poreda R. J. (2014) Noble gases identify the
762 mechanisms of fugitive gas contamination in drinking-water wells overlying the Marcellus and
763 Barnett Shales. *Proc. Natl. Acad. Sci.* **111**, 14076–14081.
- 764 Davies D. R. and Rawlinson N. (2014) On the origin of recent intraplate volcanism in Australia.
765 *Geology* **42**, 1031–1034.
- 766 Deines P., Langmuir D. and Harmon R. S. (1974) Stable carbon isotope ratios and the existence of a
767 gas phase in the evolution of carbonate ground waters. *Geochim. Cosmochim. Acta* **38**, 1147–
768 1164.
- 769 Demidjuk Z., Turner S., Sandiford M., George R., Foden J. and Etheridge M. (2007) U-series isotope
770 and geodynamic constraints on mantle melting processes beneath the Newer Volcanic Province
771 in South Australia. *Earth Planet. Sci. Lett.* **261**, 517–533.
- 772 Dixon T., McCoy S. T. and Havercroft I. (2015) Legal and Regulatory Developments on CCS. *Int. J.*
773 *Greenh. Gas Control* **40**, 431–448.

- 774 Duddy I. R. (1997) Focussing exploration in the Otway Basin: understanding timing of source rock
775 maturation. *APPEA J.* **37**, 178–191.
- 776 Giese R., Henniges J., Lüth S., Morozova D., Schmidt-Hattenberger C., Würdemann H., Zimmer M.,
777 Cosma C. and Juhlin C. (2009) Monitoring at the CO₂ SINK site: A concept integrating
778 geophysics, geochemistry and microbiology. *Energy Procedia* **1**, 2251–2259.
- 779 Giggenbach W. F., Sano Y. and Wakita H. (1993) Isotopic composition of helium, and CO₂ and CH₄
780 contents in gases produced along the New Zealand part of a convergent plate boundary.
781 *Geochim. Cosmochim. Acta* **57**, 3427–3455.
- 782 Gilfillan S., Haszedline S., Stuart F., Gyore D., Kilgallon R. and Wilkinson M. (2014) The application of
783 noble gases and carbon stable isotopes in tracing the fate, migration and storage of CO₂.
784 *Energy Procedia* **63**, 4123–4133.
- 785 Gilfillan S. M. V., Sherk G. W., Poreda R. J. and Haszeldine R. S. (2017) Using noble gas fingerprints at
786 the Kerr Farm to assess CO₂ leakage allegations linked to the Weyburn-Midale CO₂ monitoring
787 and storage project. *Int. J. Greenh. Gas Control* **63**, 215–225.
- 788 Gilfillan S. M. V, Ballentine C. J., Holland G., Blagburn D., Lollar B. S., Stevens S., Schoell M. and
789 Cassidy M. (2008) The noble gas geochemistry of natural CO₂ gas reservoirs from the Colorado
790 Plateau and Rocky Mountain provinces, USA. *Geochim. Cosmochim. Acta* **72**, 1174–1198.
- 791 Gilfillan S. M. V, Lollar B. S., Holland G., Blagburn D., Stevens S., Schoell M., Cassidy M., Ding Z., Zhou
792 Z., Lacrampe-Couloume G. and Ballentine C. J. (2009) Solubility trapping in formation water as
793 dominant CO₂ sink in natural gas fields. *Nature* **458**, 614–618.
- 794 Györe D., Gilfillan S. M. V. and Stuart F. M. (2017) Tracking the interaction between injected CO₂ and
795 reservoir fluids using noble gas isotopes in an analogue of large-scale carbon capture and
796 storage. *Appl. Geochemistry* **78**, 116–128.
- 797 Györe D., Stuart F. M., Gilfillan S. M. V and Waldron S. (2015) Tracing injected CO₂ in the Cranfield
798 enhanced oil recovery field (MS, USA) using He, Ne and Ar isotopes. *Int. J. Greenh. Gas Control*
799 **42**, 554–561.
- 800 Hand M. and Sandiford M. (1999) Intraplate deformation in central Australia, the link between
801 subsidence and fault reactivation. *Tectonophysics* **305**, 121–140.
- 802 Haszeldine R. S., Quinn O., England G., Wilkinson M., Shipton Z. K., Evans J. P., Heath J., Crossey L.,
803 Ballentine C. J. and Graham C. M. (2005) Natural geochemical analogues for carbon dioxide

804 storage in deep geological porous reservoirs, a United Kingdom perspective. *Oil Gas Sci.*
805 *Technol.* **60**, 33–49.

806 Holland G. and Gilfillan S. (2013) Application of noble gases to the viability of CO₂ storage. In *The*
807 *Noble Gases as Geochemical Tracers* Springer Berlin Heidelberg, Berlin, Heidelberg. pp. 177–
808 223.

809 IPCC (2005) *IPCC Special report on Carbon Dioxide Capture and Storage.*, UK: Cambridge University
810 Press, New York. Available at: [https://www.ipcc.ch/pdf/special-](https://www.ipcc.ch/pdf/special-reports/srccs/srccs_wholereport.pdf)
811 [reports/srccs/srccs_wholereport.pdf](https://www.ipcc.ch/pdf/special-reports/srccs/srccs_wholereport.pdf).

812 Italiano F., Yuce G., Uysal I. T., Gasparon M. and Morelli G. (2014) Insights into mantle-type volatiles
813 contribution from dissolved gases in artesian waters of the Great Artesian Basin, Australia.
814 *Chem. Geol.* **378–379**, 75–88.

815 Jeandel E., Battani A. and Sarda P. (2010) Lessons learned from natural and industrial analogues for
816 storage of carbon dioxide. *Int. J. Greenh. Gas Control* **4**, 890–909.

817 Karolytè R., Serno S., Johnson G. and Gilfillan S. M. V. (2017) The influence of oxygen isotope
818 exchange between CO₂ and H₂O in natural CO₂-rich spring waters: Implications for
819 geothermometry. *Appl. Geochemistry* **84**, 173–186.

820 King S. D. and Anderson D. L. (1998) Edge-driven convection. *Earth Planet. Sci. Lett.* **160**, 289–296.

821 Kipfer R., Aeschbach-Hertig W., Peeters F. and Stute M. 4 Noble Gases in Lakes and Ground Waters.

822 Kipfer R., Aeschbach-Hertig W., Peeters F. and Stute M. (2002) Noble Gases in Lakes and Ground
823 Waters. *Rev. Mineral. Geochemistry* **47**, 615–700.

824 Lawrence C. R. (1969) Hydrogeology of the Daylesford Mineral District with special reference to the
825 mineral springs. *Geol. Surv. Victoria, Undergr. water Investig. Rep.* **12**.

826 Lesti C., Giordano G., Salvini F. and Cas R. (2008) Volcano tectonic setting of the intraplate, Pliocene-
827 Holocene, Newer Volcanic Province (southeast Australia): Role of crustal fracture zones. *J.*
828 *Geophys. Res. Solid Earth* **113**, 1–11.

829 Liu W., Tao C., Borjigin T., Wang J., Yang H., Wang P., Luo H. and Zhai C. (2016) Formation time of gas
830 reservoir constrained by the time-accumulation effect of ⁴He: Case study of the Puguang gas
831 reservoir. *Chem. Geol.* **469**, 246–251.

832 Lyon, Boulton P. J., Watson M. N. and Hillis R. (2005) A systematic fault seal evaluation of the Ladbroke

- 833 Grove and Pyrus traps of the Penold Trough, Otway Basin. *Aust. Pet. Prod. Explor. Assoc. J.* **45**,
834 459–476.
- 835 Mao X., Wang Y., Chudaev O. V. and Wang X. (2009) Geochemical evidence of gas sources of CO₂-
836 rich cold springs from Wudalianchi, Northeast China. *J. Earth Sci.* **20**, 959–970.
- 837 Marty B. and Jambon A. (1987) C³He in volatile fluxes from the solid Earth: implications for carbon
838 geodynamics. *Earth Planet. Sci. Lett.* **83**, 16–26.
- 839 Marty B. and Tolstikhin I. N. (1998) CO₂ fluxes from mid-ocean ridges, arcs and plumes. *Chem. Geol.*
840 **145**, 233–248.
- 841 Matthews A., Fouillac C., Hill R., O’Nions R. K. and Oxburgh E. R. (1987) Mantle-derived volatiles in
842 continental crust: the Massif Central of France. *Earth Planet. Sci. Lett.* **85**, 117–128.
- 843 Myers M., Stalker L., Pejcic B. and Ross A. (2013) Tracers – Past, present and future applications in
844 CO₂ geosequestration. *Appl. Geochemistry* **30**, 125–135.
- 845 Newell D. L., Jessup M. J., Hilton D. R., Shaw C. A. and Hughes C. A. (2015) Mantle-derived helium in
846 hot springs of the Cordillera Blanca, Peru: Implications for mantle-to-crust fluid transfer in a
847 flat-slab subduction setting. *Chem. Geol.* **417**, 200–209.
- 848 O’Nions R. K. and Oxburgh E. R. (1988) Helium, volatile fluxes and the development of continental
849 crust. *Earth Planet. Sci. Lett.* **90**, 331–347.
- 850 van Otterloo J., Cas R. A. F. and Sheard M. J. (2013) Eruption processes and deposit characteristics at
851 the monogenetic Mt. Gambier Volcanic Complex, SE Australia: implications for alternating
852 magmatic and phreatomagmatic activity. *Bull. Volcanol.* **75**, 737.
- 853 van Otterloo J., Raveggi M., Cas R. A. F. and Maas R. (2014) Polymagmatic Activity at the
854 Monogenetic Mt Gambier Volcanic Complex in the Newer Volcanics Province, SE Australia: New
855 Insights into the Occurrence of Intraplate Volcanic Activity in Australia. *J. Petrol.* **55**, 1317–
856 1351.
- 857 Ozima M. and Podosek F. A. (2002) *Noble Gas Geochemistry.*, Cambridge University Press.
- 858 Price R. C., Gray C. M. and Frey F. A. (1997) Strontium isotopic and trace element heterogeneity in
859 the plains basalts of the Newer Volcanic Province, Victoria, Australia. *Geochim. Cosmochim.*
860 *Acta* **61**, 171–192.
- 861 Roberts J. J., Gilfillan S. M. V., Stalker L. and Naylor M. (2017) Geochemical tracers for monitoring

- 862 offshore CO₂ stores. *Int. J. Greenh. Gas Control* **65**, 218–234.
- 863 Robertson G. B., Prescott J. R. and Hutton J. T. (1996) Thermoluminescence dating of volcanic activity
864 at Mount Gambier, South Australia. *Trans. R. Soc. South Aust.* **120**, 7–12.
- 865 Rudnick R. L. and Fountain D. M. (1995) Nature and composition of the continental crust: A lower-
866 crustal perspective. *Rev. Geophys.* **33**, 267–309.
- 867 Ruzié L., Aubaud C., Moreira M., Agrinier P., Dessert C., Gréau C. and Crispi O. (2013) Carbon and
868 helium isotopes in thermal springs of La Soufrière volcano (Guadeloupe, Lesser Antilles):
869 Implications for volcanological monitoring. *Chem. Geol.* **359**, 70–80.
- 870 Sakamoto M., Sano Y. and Wakita H. (1992) ³He/⁴He ratio distribution in and around the Hakone
871 volcano. *Geochem. J.* **26**, 189–195.
- 872 Sano Y. and Marty B. (1995) Origin of carbon in fumarolic gas from island arcs. *Chem. Geol.* **119**, 265–
873 274.
- 874 Sano Y., Takahata N. and Seno T. (2006) Geographical distribution of ³He/⁴He ratios in the Chugoku
875 District, Southwestern Japan. *Pure Appl. Geophys.* **163**, 745–757.
- 876 Sano Y., Wakita H. and Williams S. N. (1990) Helium-isotope systematics at Nevado del Ruiz volcano,
877 Colombia: implications for the volcanic hydrothermal system. *J. Volcanol. Geotherm. Res.* **42**,
878 41–52.
- 879 Sherwood Lollar B., Ballentine C. J. and O’Nions R. K. (1997) The fate of mantle-derived carbon in a
880 continental sedimentary basin: Integration of relationships and stable isotope signatures.
881 *Geochim. Cosmochim. Acta* **61**, 2295–2307.
- 882 Sherwood Lollar B., O’Nions R. K. and Ballentine C. J. (1994) Helium and neon isotope systematics in
883 carbon dioxide-rich and hydrocarbon-rich gas reservoirs. *Geochim. Cosmochim. Acta* **58**, 5279–
884 5290.
- 885 Shugg A. (2009) Hepburn Spa: Cold carbonated mineral waters of Central Victoria, South Eastern
886 Australia. *Environ. Geol.* **58**, 1663–1673.
- 887 Smith S. P. (1985) Noble gas solubility in water at high temperature. *Eos (Washington, DC)*. **66**, 397.
- 888 Stalker L. and Myers M. (2014) Tracers—pilot versus commercial scale deployment for carbon
889 storage. *Energy Procedia* **63**, 4199–4208.

890 Teasdale J. P., Pryer L. L., Stuart-Smith P. G., Romine K. K., Etheridge M. A., Loutit T. S. and Kyan D.
891 M. (2003) Structural framework and basin evolution of Australia's southern margin. *APPEA J.*
892 **43**, 13–37.

893 Tolstikhin I. N., Ballentine C. J., Polyak B. G., Prasolov E. M. and Kikvadze O. E. (2017) The noble gas
894 isotope record of hydrocarbon field formation time scales. *Chem. Geol.* **471**, 141–152.

895 Torgersen T. (1980) Controls on pore-fluid concentration of 4He and ^{222}Rn and the calculation of
896 $4\text{He}/^{222}\text{Rn}$ ages. *J. Geochemical Explor.* **13**, 57–75.

897 Walton N. R. G. (1989) Electrical conductivity and Total Dissolved Solids—what is their precise
898 relationship? *Desalination* **72**, 275–292.

899 Watson M. N., Boreham C. J. and Tingate P. R. (2004) Carbon dioxide and carbonate cements in the
900 Otway Basin; implications for geological storage of carbon dioxide. *APPEA J.* **44**, 703–720.

901 Watson M. N., Zwingmann N., Lemon N. M. and Tingate P. R. (2003) Onshore Otway Basin carbon
902 dioxide accumulations: CO_2 -induced diagenesis in natural analogues for underground storage
903 of greenhouse gas. *APPEA J.* **43**, 637–653.

904 Wellman P. (1983) Hotspot volcanism in Australia and New Zealand: Cainozoic and mid-Mesozoic.
905 *Tectonophysics* **96**, 225–243.

906 Wellman P. and McDougall I. (1974) Cainozoic igneous activity in eastern Australia. *Tectonophysics*
907 **23**, 49–65.

908 Wilkinson M., Gilfillan S. M. V, Haszeldine R. S. and Ballentine C. J. (2009) Plumbing the Depths:
909 Testing Natural Tracers of Subsurface CO_2 Origin and Migration, Utah. In *Carbon dioxide*
910 *sequestration in geological media-State of the science* AAPG Special Volumes. pp. 619–634.

911 Williams S. N., Sano Y. and Wakita H. (1987) Helium-3 emission from Nevado Del Ruiz Volcano,
912 Colombia. *Geophys. Res. Lett.* **14**, 1035–1038.

913 Wycherley H., Fleet A. and Shaw H. (1999) Some observations on the origins of large volumes of
914 carbon dioxide accumulations in sedimentary basins. *Mar. Pet. Geol.* **16**, 489–494.

915 Zhou Z. and Ballentine C. J. (2006) 4He dating of groundwater associated with hydrocarbon
916 reservoirs. *Chem. Geol.* **226**, 309–327.

917